Final Scientific/Technical Report

DOE Award: DE-FE0007107

Project Title: Large Eddy Simulation Modeling of Flashback and Flame Stabilization in Hydrogen-Rich Gas Turbines Using a Hierarchical Validation Approach

Submitted by: Noel T. Clemens (Principal Investigator)
Professor
Dept. of Aerospace Engineering and Engineering Mechanics
The University of Texas at Austin
512-471-6773
clemens@mail.utexas.edu

Venkat Raman (co-Principal Investigator)
Associate Professor
Department of Aerospace Engineering
University of Michigan
734-764-4318
ramanvr@umich.edu

DUNS Number: 170230239

Submitted to: US DOE NETL
626 Cochrans Mill Road
PO Box 10940
Pittsburgh, PA 15236-0940

Report Date: March 18, 2016

Reporting Period: 10/01/2011 through 9/30/2015

Disclaimer

This report was prepared as an account of work sponsored by an agency of the United States Government. Neither the United States Government nor any agency thereof, nor any of their employees, makes any warranty, express or implied, or assumes any legal liability or responsibility for the accuracy, completeness, or usefulness of any information, apparatus, product, or process disclosed, or represents that its use would not infringe privately owned rights. Reference herein to any specific commercial product, process, or service by trade name, trademark, manufacturer, or otherwise does not necessarily constitute or imply its endorsement, recommendation, or favoring by the United States Government or any agency thereof. The views and opinions of authors expressed herein do not necessarily state or reflect those of the United States Government or any agency thereof.

Abstract

This project was a combined computational and experimental effort to improve predictive capability for boundary layer flashback of premixed swirl flames relevant to gas-turbine power plants operating with high-hydrogen-content fuels. During the course of this project, significant progress in modeling was made on four major fronts: 1) use of direct numerical simulation of turbulent flames to understand the coupling between the flame and the turbulent boundary layer; 2) improved modeling capability for flame propagation in stratified pre-mixtures; 3) improved portability of computer codes using the OpenFOAM platform to facilitate transfer to industry and other researchers; and 4) application of LES to flashback in swirl combustors, and a detailed assessment of its capabilities and limitations for predictive purposes.

A major component of the project was an experimental program that focused on developing a rich experimental database of boundary layer flashback in swirl flames. Both methane and high-hydrogen fuels, including effects of elevated pressure (1 to 5 atm), were explored. For this project, a new model swirl combustor was developed. Kilohertz-rate stereoscopic PIV and chemiluminescence imaging were used to investigate the flame propagation dynamics. In addition to the planar measurements, a technique capable of detecting the instantaneous, time-resolved 3D flame front topography was developed and applied successfully to investigate the flow-flame interaction.

The UT measurements and legacy data were used in a hierarchical validation approach where flows with increasingly complex physics were used for validation. First component models were validated with DNS and literature data in simplified configurations, and this was followed by validation with the UT 1-atm flashback cases, and then the UT high-pressure flashback cases. The new models and portable code represent a major improvement over what was available before this project was initiated.

Table of Contents

1 Executive Summary

In this project we have significantly improved LES modeling capability of boundary layer flashback relevant to fuel-flexible gas-turbine combustors. The validation approach taken is by validating subcomponent models first using simplified-physics systems such as jets-flames-in-crossflow or DNS of channel-flow flashback. Validation then occurs through increasingly complex systems such as flashblack with wall heat transfer, stratified flows, and low-pressure swirling flows. Final validation takes place at the top of the pyramid, using a complex multi-physics problem, which in this case is flashback of a swirl flame at elevated pressure. An important component of this work is the companion experimental study which seeks to provide validation data that are not available in the literature. The experimental program focused on measurements of flashback in a newly-developed model swirl combustor.

1.1 Experimental Program

The experimental program produced a rich database of boundary layer flashback in lean-premixed swirl flames with varying hydrogen content fuels, and at pressures ranging from 1 to 5 atm. A new model combustor was designed that included swirl vanes, a mixing tube with center body, and a primary combustion section. Turbulent, lean-premixed flames of methane and hydrogen were studied at atmospheric pressure and bulk flow velocities up to 5 m/s (16.4 ft/s). Hydrogen content ranged from 0% to 95% and equivalence ratios ranged from 0.4 to 1. The focus was on the upstream flame propagation inside the mixing tube. Stereoscopic particle image velocimetry (PIV) was applied at kilohertz-rates to provide the time-resolved, three-component velocity field. The flame front was detected simultaneously based on the acquired Mie scattering images. Simultaneous high-speed chemiluminescence imaging provided the overall flame shape and global propagation direction. In addition to the planar measurements, a technique capable of detecting the instantaneous, time-resolved 3D flame front topography was developed and applied successfully. The resulting data include the simultaneous 3D flame front and volumetric velocity field at 5 kHz.

Substantial new information about the flashback physics was developed, and this information was valuable for testing the fundamental modeling assumptions. Flashback was found to occur in the form of large-scale, convex-shaped flame tongues, which swirl in the bulk flow direction as they propagate upstream. Gas dilatation associated with the heat release was found to impose a blockage effect on the approach flow. As a result, a region of negative axial velocity forms along the leading side of the flame tongues, which facilitates the upstream flame propagation. These regions of negative axial velocity, already observed in previous studies, were shown to be the result of a 3D flow deflection as opposed to boundary layer separation or flow recirculation. The effect of hydrogen addition on flashback showed that this basic mechanism does not change for the high hydrogen content flames investigated in the present work, but quantitative differences were observed. The basic physics did not seem to change with increasing pressure, but the flame exhibited reduced radial spread rate and considerably more wrinkling of the flame surface.

1.2 Computational Modeling Program

Extensive validation of the LES models was accomplished using DNS of boundary layer flashback in turbulent channel flow at modest Reynolds number. The exercise assessed the key physical characteristics that need to be represented in order to reproduce flashback using LES computations. Investigated characteristics include subgrid flame models, surface heat loss, preferential diffusion, LES grid size and fluid compressibility,

The LES filter-widths were comparable to the smallest turbulence length scales, which would imply that the momentum description is reasonably accurate in the LES calculations. The flame, on the other hand, was approximated as a thin front using different models. It was found that the LES computations are very accurate in predicting the structure of the turbulent flame front; however, there was a discrepancy in the propagation velocity of the flame front. In other words, a slowly moving LES flame front was able to produce the structures of a faster moving DNS front. The flamelet-based models produced lesser variability to simulation conditions, including the choice of other subfilter models. It was found for the algebraic-flame-surface-density (AFSD) model that representing accurately the diffusion term was crucial to observe the characteristic flame blockage described in the DNS. A similar behavior for the depth and flashback velocity parameter was observed with coarse filtered-tabulated-chemistry for LES (F-TACLES model.

A premixed flamelet combustion approach with F-TACLES closure model was used in LES of the UT swirling burner with and without reaction. The simulations proved accurate: the mean velocity within the mixing tube matched the experimental results, despite some sensitivity to inflow boundary conditions. Furthermore, macroscopic flow features such as high-speed streaks, vortex breakdown, and a precessing vortex core were also well represented. The results obtained in the different configurations tested give good confidence about the ability of the models chosen to represent a single flashback realization. Although this confirms that most of the physics involved in a flashback event is well represented, it is not the kind of prediction expected for the computational tool. What is expected is rather related to the probability of witnessing a flashback given one operational condition.

In order to assess the prediction capability of the model regarding the flashback probability, a set of simulations was conducted starting from different initial conditions. The initial conditions were sampled based on the position of the precessing vortex associated with the swirl. Similarly, a set of experiments started at nominally the same initial conditions were conducted to investigate the variability of flashback. It turns out that the observed standard deviation of the mean flashback speed is much smaller in the simulations than in the experiments.

We can conclude that using the combustion models led to reasonably accurate prediction of flashback velocity. However, in the actual context of flashback prediction, the model was not as sensitive as the experiment to variable conditions, which indicates that the model does not accurately represent the variability associated with the event. This is an important contribution as it shows that using LES for such problems requires a careful definition of the statistics that LES can provide. Subfilter stress and scalar variance models have to be revisited for coherence with the probabilistic point of view adopted.

2 Introduction

The successful design of future lean-premixed and fuel-flexible gas turbine combustors requires an improved fundamental understanding and computational modeling capability of complex dynamical properties of the flow such as static and dynamic combustion instabilities. Static instabilities refer to the flame propagating into a section of the combustor where it is not supposed to be. Such instabilities include flame flashback and blow out. Dynamic instabilities due to the coupling between the heat release rate and acoustic pressure fluctuations can cause a mechanical failure of the combustor or trigger a static instability. Currently employed combustors, which are designed to run on natural gas, are challenged by the desire to use synthetic gases with a high-hydrogen content, which differ substantially in their chemical, transport and thermal properties. One of the key technical barriers in the development of combustors suited for operating on hydrogen-rich gas mixtures is preventing flame flashback. Flashback refers to the undesired upstream propagation of the flame from the combustion chamber into the premix section. The premix nozzles are not designed to withstand the heat load due to a flame. Sustained upstream flame propagation and flame anchoring in the preheat section is hence a serious safety risk.

Therefore, the goal of this project was to a predictive computational tool for capturing flame flashback in high hydrogen content fuels used in gas turbines. The main modeling challenge is in understanding the propagation of a turbulent flame through a near-wall turbulent boundary layer. In addition, heat transfer to the wall will cause the flame to quench very close to the wall. Since these features are unique for flame flashback triggered by boundary layers, there is no currently available technique for modeling such flows. Hence, the first objective of this work is to use direct numerical simulations to understand the coupling between the flame and the turbulent boundary layer. Since in practical combustors, the risk of flashback is mitigated with the use of fuel profiling (equivalence ratio stratification), which presents new modeling challenges. Therefore, a second objective is to develop models that enable prediction of stratification effects. The final objective has to deal with what we term as modeling portability. Although significant progress has been made over the last decade on the simulation of complex reacting flows, such advances have not been fully transferred to industry and industrial researchers. We have addressed this shortcoming in our modeling framework.

The modeling effort was accompanied by an experimental validation effort. The goal of the experimental effort was to provide a rich experimental database that would aid in validation of the LES models. Furthermore, the experiments were intended to aid in the understanding of the physics of boundary layer flashback because improved knowledge of the physics can inform fundamental modeling assumptions. The experimental effort involved the development of a model swirl combustor with premix section and combustor. The premix section used a center body configuration so the flame flashed back along the center body wall. Flashback in this combustor was studied using high-speed chemi-luminescence imaging and high-speed PIV. Both planar PIV and tomographic PIV were applied. Using the tomographic PIV data, we were able to develop a new 3Dflame front reconstruction algorithm, which enabled us to investigate the flow-flame interaction during boundary layer flashback. In addition to the 1-atm experiments, a new high-pressure facility was developed that enabled flashback experiments to be performed at pressures up to 5 atm. The primary diagnostics for these high-pressure conditions were high-speed luminosity and planar high-speed PIV. The accomplishments on both fronts are detailed in this report.

3 Experimental Methods

3.1 Swirl combustor: Design and Control

For this project a new model swirl combustor was designed and built to investigate flashback in a practical geometry. The swirl combustor features an axial swirler with attached bluff body (center body) as shown in Figure 1 allowing the investigation of boundary layer flashback of swirl flames.

The burner was operated in a fully-premixed mode in this work in which the reactants are mixed before entering the plenum. The fuel and air streams are passed through a custom-made static mixing pipe for that purpose, which houses a set of plates obstructing the flow path and inducing large-scale turbulence for intense mixing. The fuel-air mixture entered the plenum through four symmetrically arranged ports. A combination of a honeycomb section and wire-mesh elements inside the plenum ensured a clean inflow to the mixing tube.

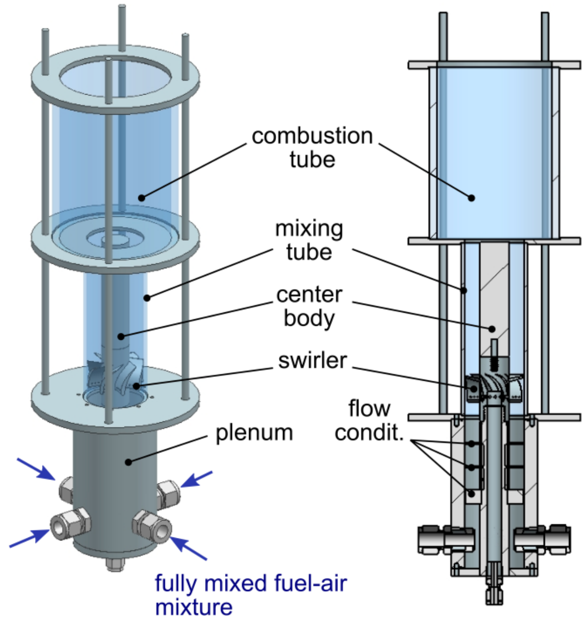

Figure 1. Schematic diagram of the model swirl combustor.

Swirl was introduced with a single axial swirler consisting of eight vanes (Fig. 2). The stainless-steel swirler was manufactured by selective-laser-melting. Each vane features six ports (three on each side), which may be used to inject fuel to operate the burner in a partially-premixed mode where fuel-air mixing occurs in the mixing tube section of the combustor as opposed to a separate mixing pipe upstream of the plenum. No fuel was injected through these ports in the low-pressure studies; however it was for high-pressure studies. The vane trailing-edges were at an angle of 60° relative to the tube axis. The swirl number is approximately $S \approx 0.9$ based on a numerical simulation of the flow field and is calculated as the ratio of axial to circumferential momentum flux based on time and space averaged radial profiles in a plane 10 mm upstream of the mixing tube exit. The hub diameter of the swirler is 25.4 mm. A stainless-steel center body, of equal diameter to the swirler hub, was attached to the swirler, ending flush with the end of the mixing tube.

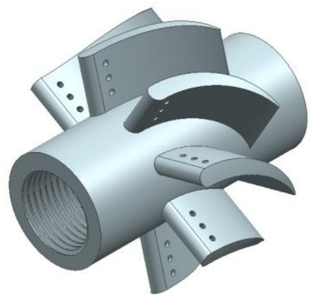

Figure 2. Solid model of the axial swirler.

The mixing tube was made of a high-optical quality quartz tube, which provides optical access for the laser diagnostics. Methane-air and hydrogen-methane-air mixtures were used as a fuel. Flashback experiments started with a stable flame in the combustion chamber. The distance between center body and flame base under stable conditions was about 10 mm, depending on flow rate and equivalence ratio. Flashback was then initiated by creating a step-change in equivalence ratio to a pre-defined value. The time from ignition to flashback was typically about 10 seconds to keep the thermal load on the combustor low.

3.2 Planar laser diagnostics

The interaction between the velocity field and the flame front is of primary interest to improve the understanding of flashback. High-speed Mie scattering imaging in a radial-axial plane served both to measure the velocity field and to detect the flame front location in this work.

3.2.1 High-speed Mie scattering imaging

The flow was seeded with olive oil droplets of approximately 1 µm diameter for measurements focusing on the velocity field in the unburnt gas. The droplets were generated with an atomizer (TSI Six-Jet-Atomizer 9306). Measurements investigating both the unburnt and burnt gas velocity fields were conducted using alumina particles (Al_2O_3) of comparable size (~1 µm), which survive at combustion temperatures.

The particles were illuminated with two high-repetition rate, diode-pumped, frequency-doubled 527 nm Nd:YLF laser (Coherent Evolution-90) operated with about 10 mJ per pulse at a repetition rate of 4 kHz. The beams were expanded and re-collimated with a plano-concave and plano-convex cylindrical lens, respectively, to form a sheet with a width of about 20 mm. A long focal length plano-convex spherical lens was used to focus the sheet. The setup is shown in Fig. 3.

The particle scattering was imaged with two high-speed CMOS cameras (FASTCAM-ultima APX) operated in forward scattering mode at a framing rate of 8 kHz and a resolution of 256 x 512 pix². The cameras were fitted with Scheimpflug adapters and Nikkor 105 mm lenses operated with an *f*/5.6 aperture. The angle between cameras and light-sheet normal was 30°.

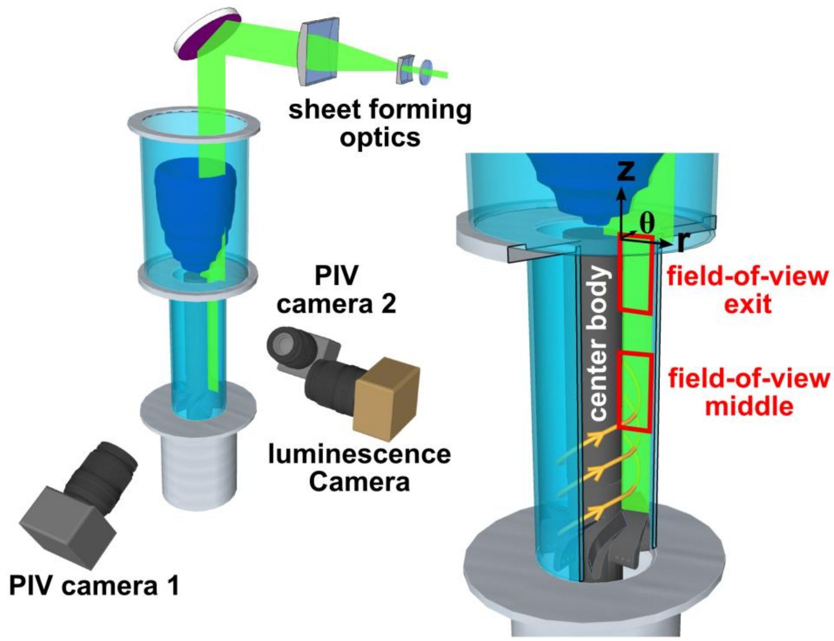

Figure 3. Diagnostic setup for simultaneous stereoscopic PIV, planar flame front detection and chemiluminescence imaging.

Measurements were taken in two different fields-of-view. The first field-of-view was positioned in the middle of the mixing tube with its top edge being located 42 mm upstream of the mixing tube exit plane (z = -42 mm). The second field-of-view was positioned with its top edge at the mixing tube exit. Both fields are 13.5 mm wide (to cover the width of the annulus) and 27 mm high with a pixel resolution of about 55 µm/pixel.

3.2.2 Stereoscopic PIV

The three-component planar velocity field was computed based on the particle image pairs recorded at 4 kHz. The time Δt_{frame} between the laser pulses of Laser 1 and Laser 2 was set to 40 µs and 80 µs for the 5.0 m/s and 2.5 m/s bulk flow velocity case, respectively. The optimal Δt_{frame} is a trade-off between uncertainty in the particle displacement and correlation loss. In the investigated swirl flow the out-of-plane velocity was on the same order as the in-plane velocity. The limiting factor in maximizing Δt_{frame} was out-of-plane correlation loss. The PIV processing was done with the LaVision software DaVis 8.2. A multi-pass cross-correlation approach with decreasing interrogation window size and window deformation was chosen in this study. The initial and final interrogation window sizes were 64 x 64 pix² and 16 x 16 pix², respectively, with 75% overlap.

3.3 Planar flame front detection

3.3.1 Evaporating oil droplets

The olive oil droplets seeded into the flow vaporized in the preheat zone serving as a marker for the flame front. A flame front extraction algorithm was developed, which was based on smoothing the particle images, and then finding the edge between the zone of particles and no-particles. An example image with detected flame front is shown in Fig. 4. The isotherm at which the olive oil used in this work vaporizes was tested in the current study to better characterize the location of the extracted interface within the flame. The olive oil droplets were measured in this study to evaporate at a temperature of about 555 K with a standard deviation of 10 K.

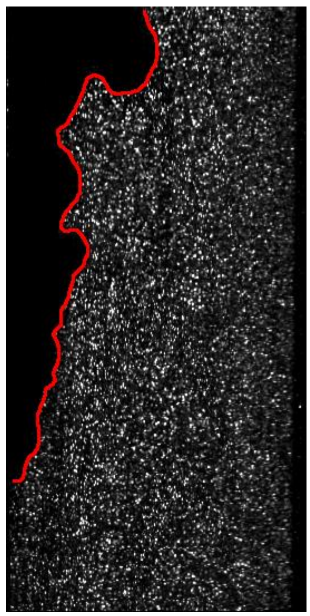

Figure 4. Flame front (red line) detection based on evaporating olive oil droplets. Hydrogen-methane-air flame (95 % hydrogen by vol., φ = 0.4).

3.4 Chemiluminescence imaging

The time-resolved flame luminescence was recorded simultaneously with all velocity measurements. The luminescence was imaged with the intensified high-speed CMOS camera Photron FASTCAM-ultima APX-i2 at 4 kHz with a resolution of 512 x 512 pix². The camera was fitted with a Nikkor 105mm lens with an f/2.8 aperture.

3.5 Three-dimensional Imaging

Boundary layer flashback of swirl flames is a transient phenomenon characterized by a highly three-dimensional flow-flame interaction. Simultaneous, instantaneous, time-resolved volumetric measurements of the velocity field and flame topography were hence desired to investigate the phenomenon. An approach based on the tomographic reconstruction of the volumetric particle field has been developed and demonstrated successfully as part of this work.

High-speed Mie scattering imaging from an aerosol seeded into the flow and illuminated with a laser was utilized to determine the three-dimensional flame topography and to measure the volumetric velocity field in the unburnt gas. The experimental setup is shown in Fig. 5. The scattering was recorded from four different views, which provides sufficient information for a tomographic reconstruction of the three-dimensional particle field. The reconstructed particle field provides the basis for the three-dimensional flame-front detection algorithm as well as tomographic PIV to obtain the volumetric velocity field.

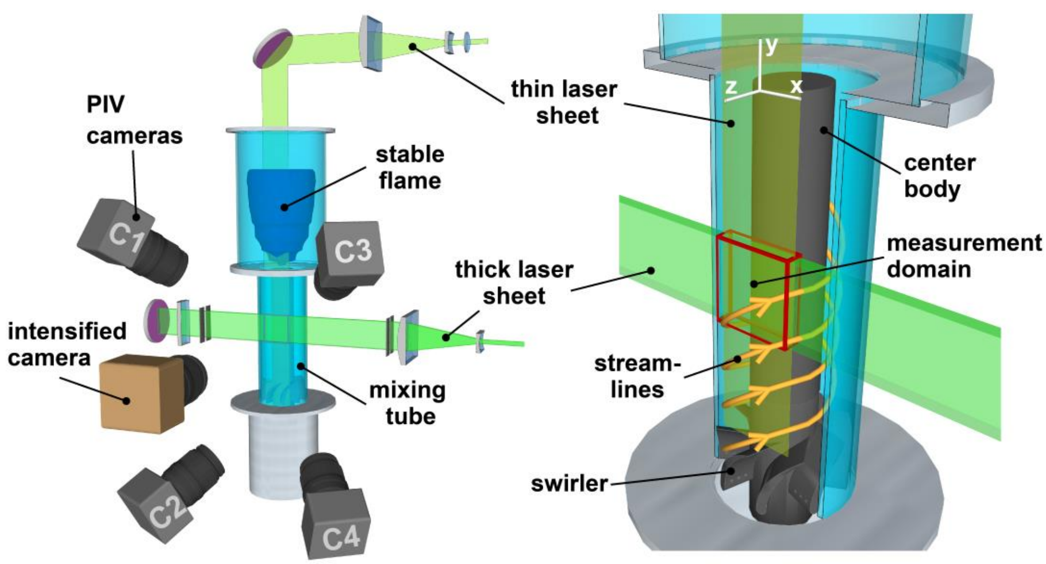

Figure 5. Diagnostic setup for 3D flame front detection and tomographic PIV.

The measurements were conducted in a volume close to the center body wall about half way between the swirler and mixing tube exit. The thick sheet entered the mixing tube with a gap between it and the center body of about 0.8 mm to reduce background illumination, which primarily results from secondary scattering off the center body wall when illuminating the droplets. The scattered light intensity off the center body is not isotropic and depends on the polarization of the incoming light.

4 Results and Discussion

4.A Experimental Program: Flashback at 1 atm

Most of the experimental program focused on measurements at 1 atm because higher fidelity measurements were possible. These measurements made up the bulk of the validation cases. A select number of cases were conducted at pressures up to 5 atm and these are described in Sec. 4.B.

4.A.1 Modes of Upstream Flame Propagation

A significant amount of new insights have been learned in this study regarding the propagation of a turbulent flame into a swirling boundary layer. These insights were made possible owing to the advanced diagnostics that we were able to apply to this flow. The flame propagation behavior is detailed in the following sections.

4.A.1.1 Qualitative flame shape and propagation direction

The upstream flame propagation during a flashback event is first discussed qualitatively based on high-speed chemiluminescence movies. The luminescence of a CH_4-air flame undergoing flashback at $Re_h = 4{,}000$ and $\phi = 0.7$ is shown in Figure 6 at selected time steps taken from a movie sequence recorded at 2 kHz. The time t_0 corresponds to the instant when an increase in flame luminescence is first detected visually. This increase in luminescence immediately precedes flashback. The flow swirls in the counter-clockwise direction as indicated by the red arrows. The flame tongue leading the flashback is convected with the bulk flow in the azimuthal direction as it propagates upstream along the center body wall (indicated by the blue arrows in the first two time steps). We use the term "flame tongue" rather than "flame front" to emphasize that the leading part of the flame is a protuberance or large bulge rather than an azimuthally-uniform flame surface. At t_0 + 257 ms, for instance, the flame tongue is on the back side of the center body but no portion of the flame propagates upstream on the front side. The characteristic shape of the leading flame tongues and their swirling motion in the direction of the bulk flow as they propagate upstream holds for all flames and flow rates investigated as part of this work (tens of individual flashback events). Presented chemiluminescence image sequences during flashback in a similar configuration appear to support these observations (Nauert et al., 2007; Karimi et al., 2015).

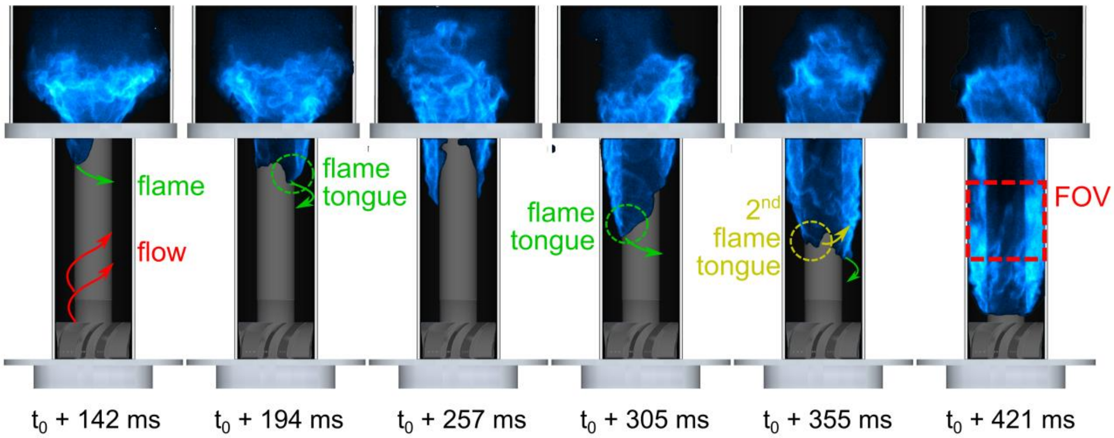

Figure 6. Chemiluminescence images at selected time steps of a CH4-air flame during flashback recorded at 2 kHz.

Additional large flame tongues may form on either side of the leading flame tongue as is seen for example at t_0 + 355 ms where the leading flame tongue is on the right side of the center body and a secondary flame tongue has formed and swirls into the field-of-view on the left (circled with a yellow line). However, only one large flame tongue is found to prevail during flashback events under most conditions; either the originally leading one continues to lead the flashback or a newly formed one is taking over. Additional flame tongues are typically washed downstream and only coexist for longer periods of times if they form rather far away from the leading flame tongue in the azimuthal direction, which suggests that conditions are not favorable for upstream flame propagation immediately to the left or right of a leading flame tongue.

The shape and propagation direction of flame tongues is investigated in more detail for a CH_4-air flame (Figure 7a) and an H_2/CH_4-air flame (Figure b). The field-of-view is shown in red in the last time step of Figure 6. We focus on a region about half way down the mixing tube to investigate the sustained upstream flame propagation in a region where the flow field is not affected by geometry-dependent mixing tube entry or exit effects. In Figure 7a and Figure 7b, at time t_1, the leading flame tongue is swirling around the center body into the field-of-view as indicated by the green arrow. The nominal flow direction is indicated by the red arrow. The edges of the center body are outlined by the vertical grey lines. We again refer to the rather large portion of the flame that is leading the flashback as a flame tongue as indicated for both flames at time t_2. In contrast, we refer to smaller structures along the flame front as flame bulges. Such flame bulges tend to form on the trailing side of the flame tongue. Flame tongues and flame bulges, as defined in this work, may be differentiated quantitatively in terms of their size (width or radius of curvature), which differs by an order-of-magnitude. Flame tongues have a characteristic size on the order of the geometry of the mixing tube (diameter of the center body or 20-30 mm) since they describe the asymmetry of the overall flame front along the circumference of the center body. Instead, flame bulges have a characteristic width on the order of 2 to 3 mm and are hence comparable in size with the measured integral scale of turbulent structures in the investigated flow.

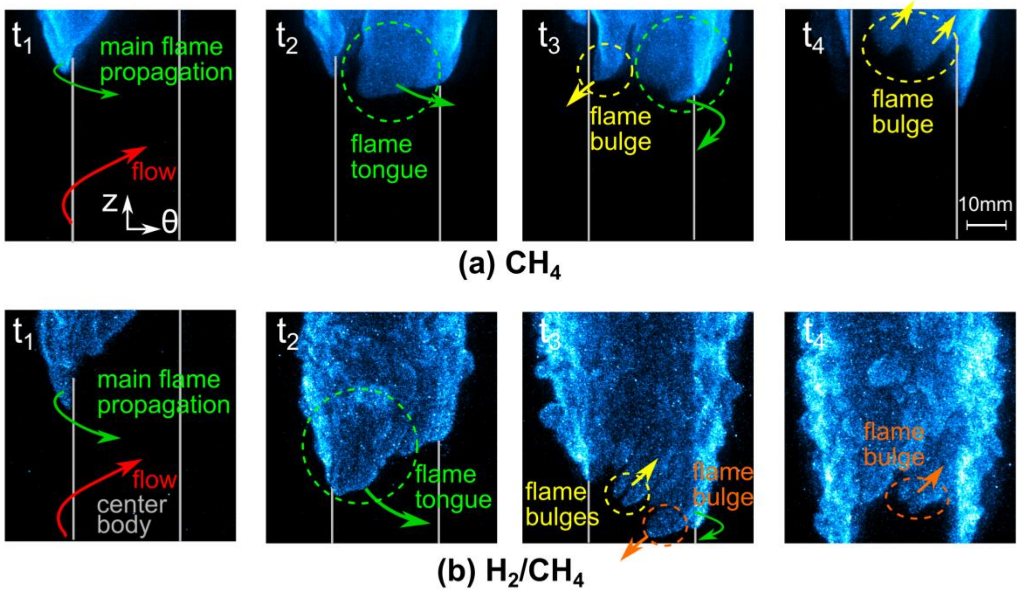

Figure 7: Chemiluminescence image sequence showing the upstream flame propagation and flame structure of a (a) CH_4-air flame, and (b) H_2/CH_4-air flame.

In the case of the methane flame (ϕ = 0.8), flame bulges form occasionally with an example seen in Figure 7a at time step t_3 and highlighted by the yellow dashed circle. This bulge attempts to propagate upstream in the negative streamwise direction as indicated by the yellow arrow and manages to momentarily resist the approach flow – it remains at a fixed location in space for about 3 ms – while the tip of the leading flame tongue continues to swirl upstream (green arrow). However, the bulge then breaks into two smaller bulges – likely due to the arrival of a faster moving flow structure – and is convected downstream as seen 6.25 ms later at time t_4. While the flame bulge fails to initiate sustained upstream flame propagation, the tip of the leading flame tongue continues to swirl upstream as indicated by the green arrows at time steps t_2 and t_3. By time step t_4 it is on the back side of the center body.

The H_2/CH_4-air flame (95 % hydrogen by volume, ϕ = 0.4) shown in Figure 7b has the same laminar flame speed but a significantly lower flame temperature as the previously discussed methane flame but features a more convoluted flame surface, which may be attributed to thermo-diffusive effects (Law & Sung, 2000). The overall shape of the flame during flashback, however, is again characterized by a large flame tongue leading the flashback as seen at times steps t_1 and t_2. The formation of small-scale bulges located on the trailing side of the leading flame tongue and aligned with the nominal streamwise direction are more frequently observed for high-hydrogen content flames compared to the previously discussed methane flames. Furthermore, the bulges are smaller in size and manage to not just resist the approach flow (freeze at a fixed location in space) but sometimes even counter propagate into the approach flow for short distances (~1 mm), which may be attributed to a smaller quenching distance and an increase in flame speed at the tip of these convex shaped bulges owing to local enrichment effects of the deficient reactants. Based on the full movie sequence, the two bulges marked by the yellow circle at time step t_3 are being convected downstream whereas the bulge marked by the orange circle manages to counter propagate into the approach flow for a short time (~1 ms) and distance. About 11 ms later (time step t_4), this same bulge is seen (again marked by an orange circle), but now broken into two separate bulges and again washed downstream as indicated by the small orange arrow. All the while, the tip of the flame tongue leading the flashback continues to swirl upstream; it is already on the right side of the center body at t_3 (indicated by the green arrow) and on the back side below the bottom edge of the field-of-view at t_4.

The formation and break-up of the small-scale bulges on the trailing side of the leading flame tongue, particularly for the H_2/CH_4-air case, agree well in size and occurrence with the observations reported by Eichler et al. (2011) investigating flashback in a (non-swirling) channel flow. This is reasonable as the trailing sides of the swirling flame tongues observed in the current work are aligned approximately perpendicular to the streamlines of the approach flow just like in a channel flashback where the flame brush is oriented perpendicular to the flow. However, the contribution of these flame bulges to facilitate the overall flashback is different. In a channel boundary layer flashback, a combination of parameters likely to include flame speed, quenching distance and density ratio (the relative importance of each of these factors is not yet fully understood) has to be above a particular threshold such that the formation, upstream propagation, break-up and downstream convection of these small-scale bulges leads to a net upstream propagation of the entire flame brush. The requirement for the flame to achieve overall flashback in a swirl flow is different, however. Instead of fighting the approach flow head-on in form of small-scale bulges, the flame is found to flashback in the form of large-scale flame tongues swirling upstream, which appears to be the path of least resistance for the flame even when flashback was triggered at an equivalence ratio significantly beyond the flashback limit.

4.A.1.2 Flame propagation associated with small-scale bulges

We compare the velocity field upstream of small-scale bulges with non-swirling channel flashback results by Eichler et al. (2011) and Gruber et al. (2012) to provide evidence that the same mechanism facilities the upstream flame propagation associated with such bulges in our swirl flow as suggested qualitatively by the time-resolved chemiluminescence imaging. The chemiluminescence image sequence in Figure 8 shows the formation of a small-scale bulge on the trailing side of a flame tongue during a CH_4-air flame flashback ($\phi = 0.8$). Results from the volumetric velocity field measurement corresponding to an instant in time when the flame bulge resists the approach flow (the local displacement speed matches the flow velocity) is shown in Figure 8a. The three-dimensional flame topography based on our marker for the preheat zone is shown in grey. The axial velocity field is shown in a secant through the annulus, which is offset from the center body by about 0.8 mm at its closest point. The white band separates positive from negative axial velocity with the region of negative axial velocity colored in blue. A reverse flow pocket, marked by the black solid line corresponding to zero streamwise velocity, exists in agreement with previous studies (Eichler et al, 2011; Gruber et al., 2012). Three-dimensional streamlines are plotted and color coded by the y-distance to indicate their location in the depth direction as indicated in Figure 8c, which is a bottom view of Figure 8a highlighting again the location of the measurement volume in relation to the center body with the back side of the measurement domain slightly offset from the center body wall.

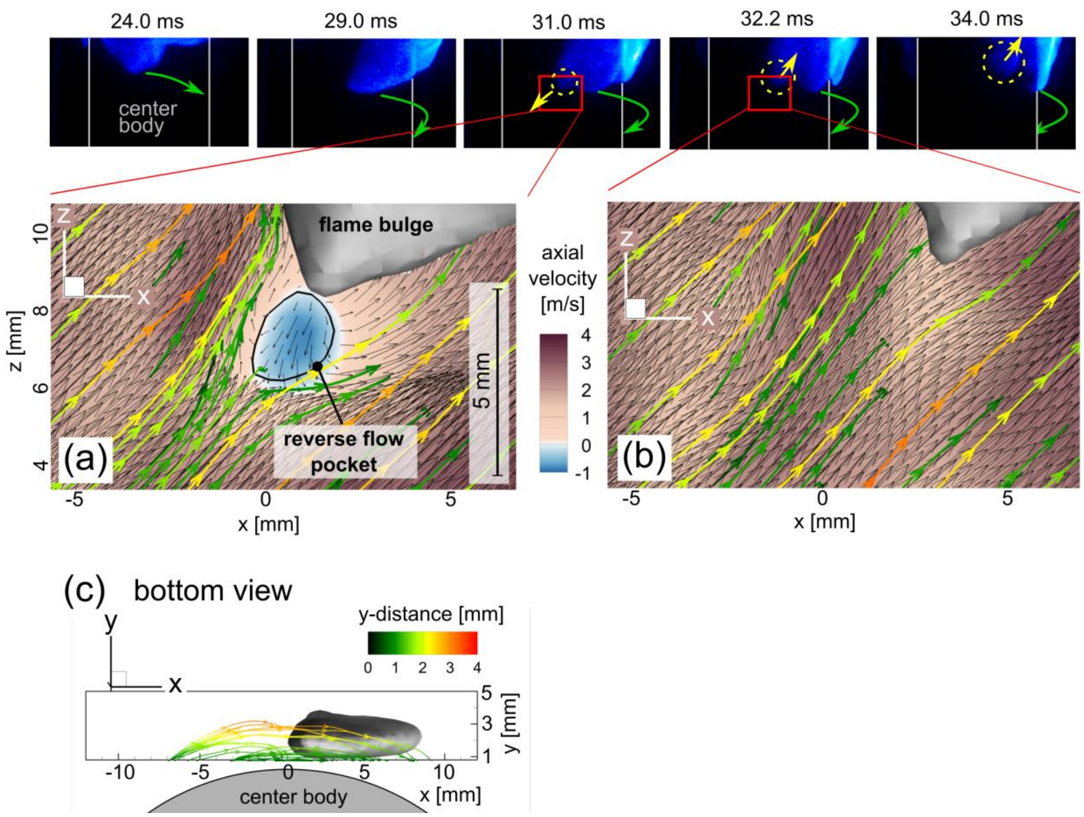

Figure 8. Formation of a small-scale flame bulge on the trailing side of a flame tongue (luminescence image sequence, top row). Axial velocity field in *y* = 0.8 mm plane and 3D streamlines showing (a) the reverse flow pocket associated with the flame bulge as it resists the approach flow and (b) the recovered flow field subsequently convecting the bulge downstream. Streamlines are colored by *y*-distance from the center body as explained in (c).

Flame bulges locally push the low-momentum near-wall fluid upstream in the negative streamwise direction, which leads to a stagnation point at the upstream end of the reverse flow pocket. The near-wall streamlines (green) diverge symmetrically to either side of the flame bulge. Streamlines farther offset from the wall (yellow and orange) still diverge but to a lesser extent. The agreement in the velocity field with the DNS results by Gruber et al. suggests that the propagation mechanism associated with these small-scale bulges is indeed the same. The DNS was further able to show that the reverse flow pockets are associated with a localized pressure peak ahead of the convex shaped bulges whereas the pressure drops downstream of the flame brush. The location where convex shaped bulges form was found to be correlated with the occurrence of low-momentum streaks (Gruber et al., 2012) as previously suggested by Eichler et al. (2011). It appears that in our swirl flow the formation of small-scale bulges is also linked to the arrival of low-momentum fluid either due to low-momentum streaks in the boundary layer or due to wake effects originating from the swirler vanes. However, since we cannot measure the velocity along the circumference of the center body but only in a tangent or wall-normal plane, we cannot establish the correlation with certainty. As described before, small-scale bulges are found not to sustain in our swirl flow and are washed downstream shortly after their formation as shown in Figure 8b.

4.A.1.3 Flame propagation associated with large flame tongues in swirl flows

Region of negative axial velocity

Regions of negative axial velocity upstream of the leading flame front have first been observed by Heeger et al. (2010) in a similar swirl burner configuration featuring a mixing tube with center body along which the flame propagates during flashback. The planar two-component velocity field in a radial-axial slice was measured in their work while simultaneously recording the flame luminescence from a point-of-view perpendicular to the planar measurement domain. Apparent upstream propagation without negative axial velocity was observed in about half of the recorded cases. The possibility that such cases correspond to instances when the laser sheet slices through the leading or trailing side of a flame tongue rather than the leading tip was suggested.

Our measurements consistently show that upstream propagation without a negative axial velocity region is an artifact associated with a planar measurement in a 3D flow in agreement with the suggestion by Heeger et *al*. (2010) As an example, a few selected time steps of a methane-air flashback ($\phi = 0.8$) movie are shown in Figure 9. The luminescence is shown in the top row with arrows indicating the nominal flow direction and the flame propagation direction as well as the PIV measurement domain (green vertical line). The corresponding velocity fields are shown in the bottom row with the grey vertical bar on the left indicating the location of the center body wall and the red line indicating the flame front (based on the employed marker for the preheat zone). The planar velocity field and flame front location measurement by itself would suggest that flashback is characterized by an initial flame propagation away from the wall (Figure 9b) followed by flame propagation along the wall without a region of negative axial velocity upstream of the flame base (Figure 9c) and finally upstream flame propagation with a region of negative axial velocity (Figure 9d). In contrast, the flame luminescence reveals that the apparent upstream propagation is instead a swirling motion as previously discussed where the flame is behind the center body in Figure 9a and the measurement slices through a downstream portion of the flame in Figure 9b and Figure 9c. Only Figure 9d corresponds to a time step when the flame tip is in the planar field-of-view. We confirmed all findings just discussed based on planar measurements with high-speed volumetric measurements to be discussed in the subsequent sections. Studying certain aspects of the three-dimensional flame-flow interaction during swirl flame flashback is therefore possible if some means to unambiguously interpret the planar data is available such as luminescence imaging from a perpendicular point-of-view in this case. True upstream propagation of the leading flame tip is found always to be associated with a region of negative axial velocity ahead of the flame tip for all conditions and all runs conducted as part of our work.

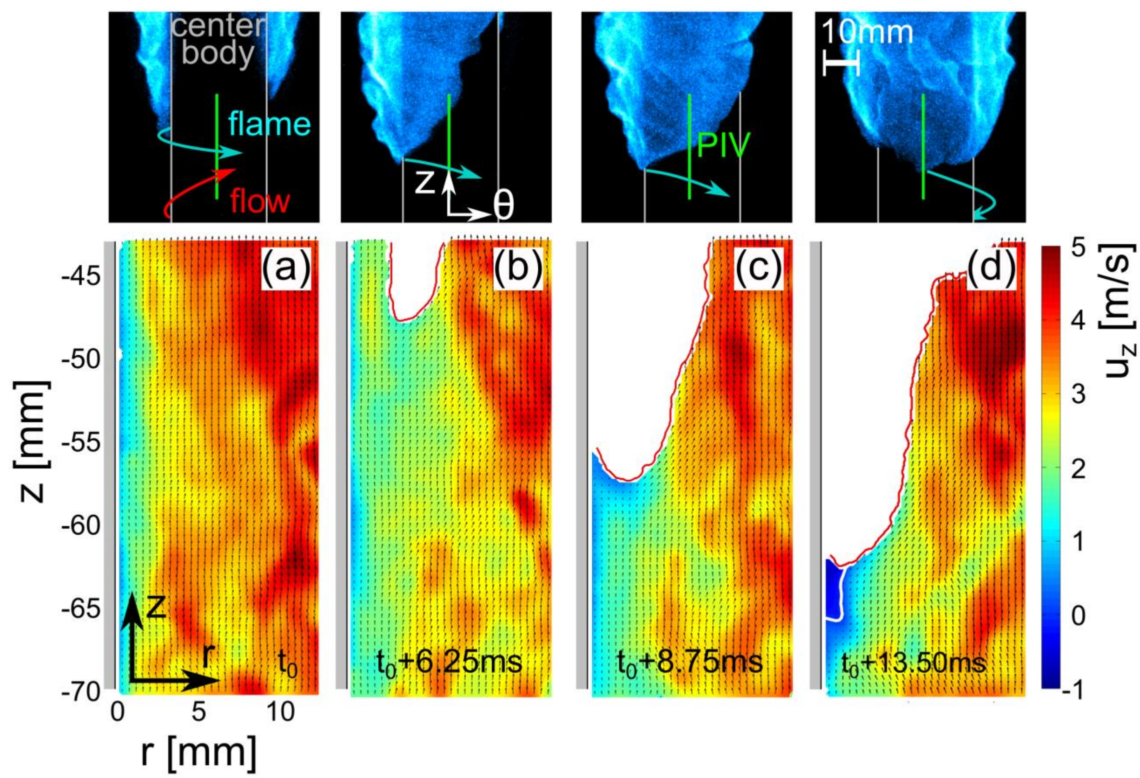

Figure 9. Simultaneous chemiluminescence (top row) and velocity field measurement (bottom row) highlighting the difference between apparent and true upstream flame propagation and its correlation with a region of negative axial velocity. The planar flame front (red line) and axial velocity field is shown in a radial-axial slice corresponding to the green line in the luminescence images. The white line in (d) is an isoline of 0 m/s indicating the region of negative axial velocity.

The region of negative axial velocity upstream of the leading flame tongue is found to exist not only immediately at the flame tip but also on its leading side corresponding to the fluid region the flame is propagating into as shown in Figure 10a.

On the leading side of the flame tongue negative axial velocity is observed in the near vicinity of the flame front only. In contrast, the region of negative axial velocity reaches far upstream in the vicinity of the flame tip as shown in Figure 10b. The length-scale of this negative axial velocity region is about 5 to 10 mm in extent based on observations from ten flashback events. This observation of the extent of negative axial velocity holds even for more turbulent conditions (twice the bulk flow velocity corresponding to Re_h = 8,000).

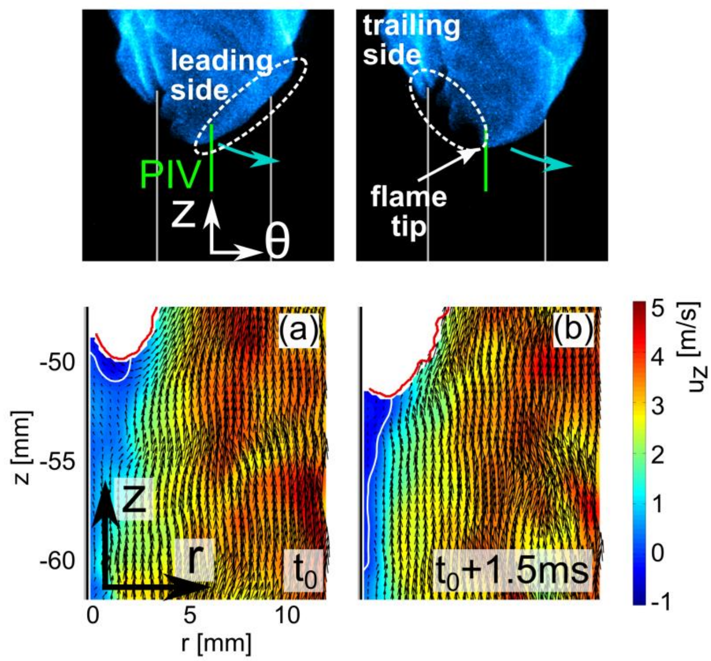

Figure 10. Velocity field and region of negative axial velocity (white line) in the vicinity of the leading flame front (red line) in a slice through the leading side of the flame tongue (a) and through the flame tip (b).

As discussed above, the investigated H_2/CH_4-air flames (95% hydrogen by volume, ϕ = 0.4) are found to be more convoluted as a result of small-scale bulges, which form more frequently compared to the methane-air flames. However, focusing on the similarities in this chapter, the upstream flame propagation again occurs in form of larger flame tongues. The velocity measurements show regions of negative axial velocity upstream of the leading flame tongue, which compare well with the findings in methane-air flames. The observed axial extent of the negative axial velocity region appear to be smaller (about 5 mm), but a wider range of conditions would need to be tested before more general conclusions can be drawn.

Three-dimensional velocity field in the vicinity of leading flame tongues

The volumetric velocity field in the vicinity of flame tongues, which dominate boundary layer flashback in the investigated swirl flames, is shown in Figure 11. The axial velocity field is seen in a secant through the annulus, as shown in Figure 5, which is offset from the center body by about 0.8 mm. The blue colored region bounded by the white band shows a region of negative axial velocity. The color coding for the three-dimensional streamlines indicates the *y*-distance from the center body. The chosen instant in time captures the tip of a larger flame tongue that is swirling with the bulk flow velocity in the counter-clockwise direction as it propagates upstream, which corresponds to the flame motion found to lead flashback in the investigated swirl flames. The velocity field is fundamentally different compared to the velocity field upstream of small-scale bulges as presented in Figure 8. The region of negative axial velocity is merely the result of a rather large-scale deflection of streamlines as opposed to a localized reverse flow pocket, which is emphasized by the near-wall streamlines (green) deflected around the tip of the flame tongue without being reversed. The azimuthal velocity component remains large upstream of the flame tongue in contrast to the reverse flow pockets which are the results of both negative axial and negative azimuthal velocity. Note that we define "reverse flow" as a region with fluid that flows counter to the dominant upstream flow direction. In the case of a swirling flow, reverse flow propagates in the negative swirl direction. A moderate level of deflection of streamlines in the investigated swirl flow is sufficient to result in a region with a negative axial component, but without flow reversal.

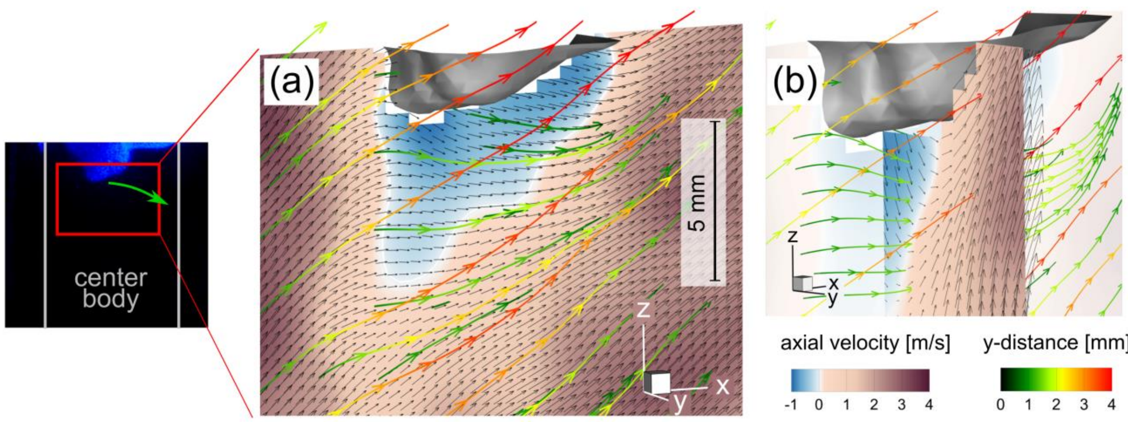

Figure 11. Three-dimensional velocity field associated with flame tongues (grey surface): (a) Axial velocity field in *y* = 0.8 mm plane and 3D streamlines. (b) Velocity field in *x* = 0 plane. Shown here: CH_4-air flame (φ = 0.8).

The velocity field is shown in a perpendicular plane in Figure 11, which corresponds to a radial-axial slice typically measured with a planar technique as presented previously in Figure 9 and Figure 10. The tangent vectors suggest flow recirculation, which has been interpreted as boundary layer separation in previous works (Heeger et al., 2010). However, neither flow recirculation nor boundary layer separation occurs upstream of the preheat zone in this case as the volumetric measurements reveal. Furthermore, the location where the velocity vectors switch from a positive to a negative axial component at the upstream end of the negative axial velocity region is not a stagnation point but instead corresponds to purely swirling flow. A stagnation point may still exist inside the burnt gas, however.

The volumetric measurement readily provides the explanation for the difference in characteristic shape and axial extend of the negative axial velocity region between the leading side of the flame tongue and at the flame tip as observed previously in planar measurements shown in Figure 10. Instead of diverging to either side of the flame tongue, the flow is deflected downwards ahead of the flame tongue as well as alongside the leading side of the flame tongue, hence providing a region of negative axial velocity for the flame to propagate into.

Fluid farther out in the radial direction is only moderately deflected in the axial direction as the streamlines colored in red indicate (Figure 11). Hence, a shear layer forms between the near-wall layer of fluid with a predominantly swirling motion and fluid away from the wall moving at a swirl angle closer to the nominal angle and hence with a significant axial component. The shear layer consists of negative azimuthal vorticity, which may also be measured with planar PIV in a radial-axial slice as shown in Figure 12. The red line marks the location of the flame front. The grey vertical line along the left edge indicates the location of the center body wall. The shear layer is indicated by the dashed black line. Figure 12a corresponds to the time step shown in Figure 10a, at which the leading side of the flame tongue is in the field of view. Negative azimuthal vorticity is concentrated in the near vicinity of the flame front. The flame continues to swirl into the measurement plane, which is associated with shear appearing farther upstream of the flame. Figure 12d corresponds to the instant in time shown in Figure 10b when the laser sheet cuts through the flame tip. At this time, a strong shear layer exists between the near-wall fluid with a negative axial velocity and fluid moving in the positive axial direction farther away from the wall.

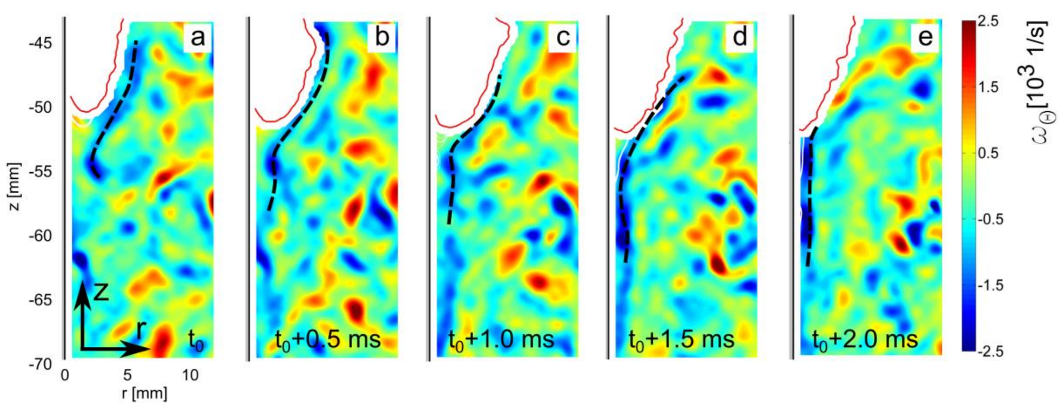

Figure 12. Azimuthal vorticity field in a radial-axial slice in the vicinity of a flame tongue (red line marks flame front) leading flashback. The black dashed line highlights a layer of vorticity moving coherently based on the movie sequence.

The production of negative azimuthal vorticity at the flame tip due to baroclinic torque, which results from the axial density gradient across the flame tip and the radial pressure gradient due to the swirl flow, has been proposed as a mechanism enhancing the flame speed along a vortex axis (Ashurst, 1996). The concept of vorticity produced by baroclinic torque and inducing a negative axial velocity has subsequently been identified as a mechanism driving flashback in the core of swirl flows associated with combustors not featuring a center body in the mixing tube (Konle et al., 2008; Konle & Sattelmayer, 2009, Kiesewetter et al., 2007). Our measurements suggest that in *boundary layer* flashback of swirl flames the observed negative azimuthal vorticity present in the immediate vicinity of the flame tip is part of a larger coherent shear layer, which reaches far upstream into the cold approach flow and hence is not dominated by vorticity production due to baroclinic torque. The data hence suggest that the observed azimuthal vorticity is not the cause but an effect of the upstream flame propagation. The observed concentration of elevated azimuthal vorticity may be the result of already existing boundary layer vorticity, which is being reoriented and transported away from the wall by the modified flow field in the vicinity of the leading flame tip. Additional vorticity may possibly be produced at the center body wall due to a pressure gradient induced by the presence of the flame tongue.

Region of influence of the local blockage effect

As described in the previous section and highlighted in Figure 11, flame tongues decelerate and deflect the approach flow. The effect flame tongues have on the approach flow may hence be described as a blockage effect due to the gas dilatation associated with the heat release. It is instructive to investigate where and how the velocity field is influenced at various points relative to a flame tongue. For that purpose time traces of axial velocity, azimuthal velocity and swirl angle (angle between the axial direction and the instantaneous, local streamwise flow direction) are evaluated at two points in space as shown in Figure 13. Both points are located at the same axial location as marked by a white cross in the sequence of chemiluminescence images shown in Figure 13a, which provides the flame location in relation to the measurement points. The instantaneous velocity evolution (thin lines) are low-pass filtered (thick lines) to highlight trends due to the presence of the flame as opposed to turbulent fluctuations.

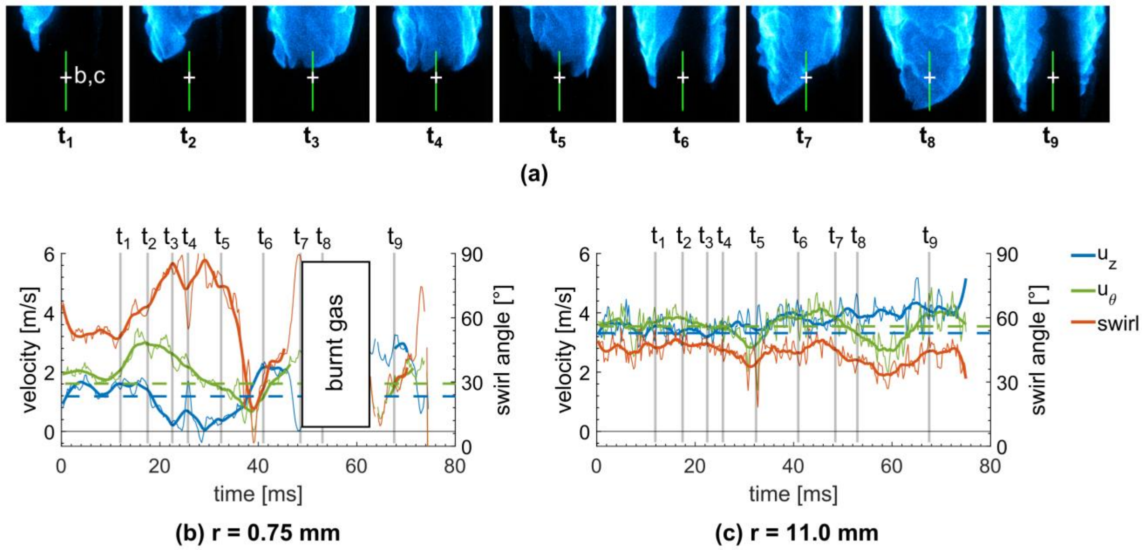

Figure 13. Time traces of axial velocity (blue), azimuthal velocity (green) and swirl angle (red) at two radial locations (b) in the boundary layer close to the center body and (c) close to the mixing tube wall, respectively. Mean velocities are marked by horizontal dashed lines. The global flame position in relation to the measurement points (white cross, same axial location) is shown in (a) at nine instants in time.

We first discuss the velocity evolution at the measurement point close to the center body wall (Figure 13b). As the flame tongue swirls through the laser plane the approach flow is decelerated starting at time t_2 and subsequently recovers again starting around time t_5 indicating that the presumed elevated pressure causing the flow deflection is limited to the portion of the annulus occupied by a flame tongue. Interestingly, the cusp between the leading flame tongue and a secondary flame tongue is associated with the immediate spike in axial velocity at time t_4. The flame tongue furthermore accelerates the azimuthal velocity on its leading side (time t_2) and decelerates it on its trailing side (time t_6). Interestingly, the same acceleration and deceleration is observed rather far downstream of the leading flame tip. At time t_7, immediately before the flame front arrives, the azimuthal velocity is high. In contrast, the azimuthal velocity is low between the time the trailing side of the flame tongue passes through and t_9. These observations suggest that the presumed region of elevated pressure is not limited to the immediate vicinity of the leading flame tip. The described velocity pattern leads to predominantly swirling motion of the near-wall fluid ahead of the flame tongue (swirl angle of about 90° between times t_2 and t_5) and a primarily axial fluid motion on the opposite side of the flame tongue. The low swirl and high axial velocity around times t_6 and t_9 indicates a reliving effect away from the flame tongue.

The second measurement point is close to the mixing tube wall and outside the burnt gas for all times show in Figure 13c. The decrease in azimuthal velocity starting around times t_5 and t_8 indicate the blockage effect of the flame tongue affects the flow close to the center body wall but also the incoming swirl flow beyond the radial portion occupied by burnt gas. The steady increase in axial velocity relative to the mean velocity (dashed line) close to the outer wall as the flame tongue swirls upstream further indicates an additional relieving affect for the unburnt gas. It appears that the path of least resistance for the flame to flashback is not to block the flow in the entire annulus or even transiently back-pressurize the entire flow, but only locally ahead of flame tongues.

A recent study was able to measure a static pressure rise on the center body wall inside the burnt gas region of a flame tongue swirling past the measurement port (Karimi et al., 2015). Our velocity field measurements further suggest that this increase in pressure is not limited to a region close to the center body wall and in addition has a magnitude capable of causing a time-rate-of-change in momentum associated with the changes in the velocity field just discussed.

4.A.1.4 Differences and similarities of propagation modes

Evidence for the existence of two different modes of upstream flame propagation along a wall during swirl flame boundary layer flashback has been presented. We now want to summarize the important features associated with each mode of flame propagation and discuss similarities as well as differences. The first mode consists of large-scale flame tongues swirling in the bulk flow direction as they propagate upstream along the center body wall and illustrated in Figure 14a. This form of flame propagation is found to lead swirl-flame boundary-layer flashback under the conditions investigated in our work. The second mode consists of small-scale bulges aligned with the streamwise direction, which may counter-propagate into the approach flow and illustrated in Figure 14b.

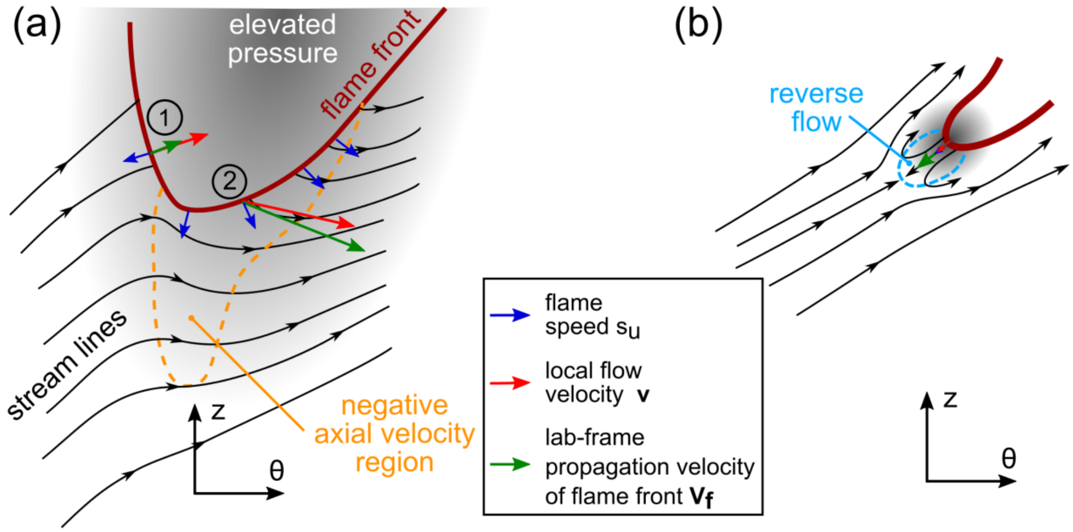

Figure 14. Schematics summarizing flame shape, flame propagation direction and important flow features associated with (a) flame tongues leading boundary layer flashback in swirl flows and (b) flame bulges counter-propagating into the approach flow on the trailing side of flame tongues.

Boundary layer flashback in non-swirling channel flows has been found to be driven by small-scale bulges, which are correlated with the arrival of low-momentum streaks in the turbulent boundary layer (Eichler & Sattelmayer, 2011; Gruber et al., 2012). Interestingly, we find that the formation of small-scale bulges in our swirl flow is only observed on the trailing side of the larger flame tongues where the flame surface is oriented perpendicular to the streamwise flow direction and hence provides the same alignment as in a 2D flow. The formation on the trailing side is likely assisted by the overall deceleration of the flow in that region due to the flame tongue itself. The formation, counter-propagation, break-up and downstream convection of small-scale bulges leads to a net upstream propagation of the flame brush in the negative streamwise direction in a channel flashback (Eichler & Sattelmayer, 2011), which is not the case for the conditions investigated in our work. In contrast, the large flame tongues leading flashback in our model swirl combustor do not depend on the arrival of low-momentum fluid, which leads to a continuous, rather than intermittent, upstream propagation of the leading flame tip. The bulges may nonetheless contribute to flashback by additionally modifying the approach flow in the vicinity of the flame tip at occasions when they are formed at the tip of the flame tongue. Furthermore, they may modify the rate at which reactants are consumed by the flame tongue by increasing the flame surface area. Whether the consumption rate and hence the rate at which low density burnt gas is generated (generation of volume) is a dominant affect for the flashback mechanism requires further investigations, however.

Both modes of flame propagation have in common that they are coupled with the velocity field through the pressure field. Both propagation modes lead to a region of negative axial velocity ahead of the leading flame tip and hence enable flashback by strongly modifying the approach flow. However, the region of negative axial velocity is the result of a different underlying velocity field. In the case of flame tongues, the approach flow is deflected in the negative axial direction as indicated by the streamlines in Figure 14a such that a predominantly swirling fluid motion with a small negative axial component exists upstream of the flame tip. No stagnation point exists upstream of the preheat zone in this case. As discussed previously, the velocity field is modified far upstream and downstream of the leading flame tip as well as beyond the burnt gas region in the radial direction, which suggests that a large portion of the burnt gas is associated with elevated pressure as indicated by the grey area in Figure 14a. In contrast, the region of negative axial velocity upstream of small-scale bulges is the result of flow reversal in a small pocket ahead of the convex shaped flame tip with a stagnation point at its upstream end as sketched in Figure 14b. The DNS has shown that the elevated pressure is restricted to the immediate vicinity of the tip of convex bulges and subsequently decreases in the burnt gas (Gruber et al., 2012), which is indicated by the grey spot in Figure 14b.

The newly found velocity field associated with flame tongues causing the observed flame propagation during swirl-flame flashback is summarized in more detail based on two locations along the flame front, positions 1 and 2, in Figure 14a. The azimuthal velocity is decreased on the trailing side of the flame tongue corresponding to a decrease in azimuthal momentum of the approach flow as indicated by the red arrow at position 1. In contrast, the azimuthal velocity is increased towards the leading side (position 2) suggesting the flame tongue is pushing the flow ahead of itself. The red arrows are drawn to scale based on the velocity field measurement. The axial velocity along the leading side is found to be negative or at least significantly decelerated even far downstream of the flame tip. The displacement speed associated with the flame front is indicated by blue arrows assuming a flame speed of 0.7 m/s. The vector sum of local flow velocity and flame speed is indicated by the green arrows providing the propagation direction and speed of a local flame front element. The discrepancy in the azimuthal flame front propagation velocity between position 1 and 2 leads to the characteristic spreading of the flame tongue in the azimuthal direction with downstream distance. The positive axial component on the trailing side indicates that flame front elements are convected downstream in agreement with the high-speed chemiluminescence movies, which show structures along this side of the flame tongue being convected downstream by the flow. In contrast, the leading side of the flame tongue continuously propagates into a region of negative axial velocity that it created by pushing the flow ahead of itself.

4.B Experimental Program: Flashback at Elevated Pressure

The present work investigates the boundary layer flashback in premixed flames of methane and air at elevated pressures. We employ high speed stereoscopic PIV and simultaneous chemiluminescence imaging to visualize the flame- flow interactions in the mixing tube during the flashback. Experiments are run at different pressures ranging from 1 to 5 atm in a new optically accessible high pressure combustion facility, shown in Fig. 15a. The middle section of this chamber is designed to optimize the optical access for stereoscopic PIV measurements. This chamber also features a window on the top flange which allows laser sheet entry from the top. A model dump combustor with an axial swirler in line with its center-body is used to stabilize the swirl flames. A step increase in equivalence ratio of premixture is used to initiate the flashback. The boundary layer flashback occurs with a large flame tongue swirling around the center-body which propagates upstream until it stabilizes in the wake of swirler vanes. This phenomenon involves a complex three dimensional flow-flame interaction which is a matter of active research (Ebi & Clemens, 2014). At higher pressures, critical parameters for boundary layer flashback like quenching distance and boundary layer thickness decreases for a given axial velocity of flow stream. In addition, corrugation of flame front at higher pressures leads to higher turbulent flame speeds which ultimately affect the stability of swirl flames. This study aims to provide a velocimetric insight for flashback occurring at elevated pressures.

The swirl combustor consists of a plenum, a transparent mixing tube and dump combustion chamber with an area ratio of 5.3. The mixing tube is made of a quartz cylinder with a coaxial swirler (swirl number S ~ 0.9) and stainless steel center-body, as shown in Fig. 15b. Design details of this combustor can be found in previous research done by Ebi & Clemens (2014).

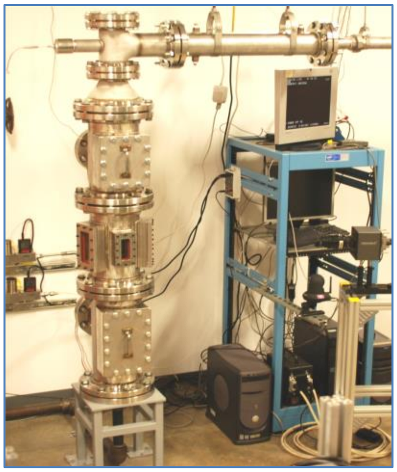

(a)

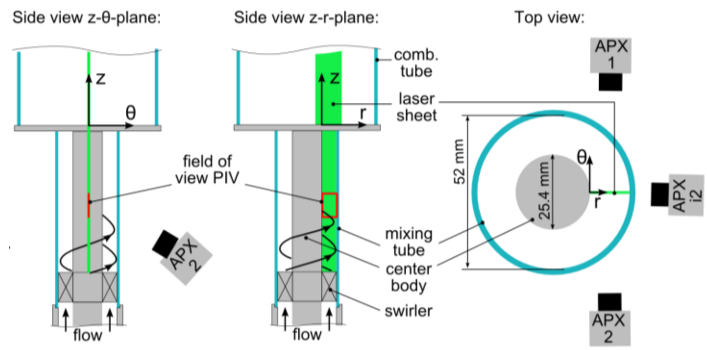

(b)

Figure 15. High pressure combustion facility. (a) photograph of the high-pressure chamber (b) schematic of the diagnostic system relative to the swirl combustor as mounted in the high-pressure chamber.

Demarcation of the flame front is important to define the region of interest in flashback experiments. High speed planar Mie scattering of laser sheet illuminated droplets (olive oil, diameter ~ 1 µm) serves dual purpose of providing PIV data and an approximate marker for flame front, owing to its evaporation in preheat region of the reaction zone. Also, the three dimensional nature of the flow field demands an overall picture to understand the out-of-plane flow features. High speed chemiluminescence images fulfill this need and assist in understanding the swirling behavior of primary flame tongue.

Time-resolved chemiluminescence images of the flame during flashback are captured with an intensified high-speed CMOS camera (FASTCAM-ultima APX-i2). The viewing direction is parallel to the laser sheet and so the field-of-view is perpendicular to the sheet as indicated in Fig. 15b. The olive oil droplets are illuminated with two high-repetition rate diode-pumped, frequency-double 527 nm Nd:YLF laser (Coherent Evolution-90) operated at a repetition rate of 4 kHz. A 20 mm wide laser sheet enters the mixing tube from the top in the r-z-plane. It is aligned with the mixing tube axis, as shown in Fig. 15b. Two high-speed CMOS cameras (FASTCAM-ultima APX) are operated in forward scattering mode at a framing rate of 8 kHz and a resolution of 256 x 512 pix^2.

Figure 16 shows the chemiluminescence snapshots taken during flashback events at different pressures for the same average axial velocity. Since the axial velocity is the same, the volumetric flow rate is also the same but the mass flow rate is higher at higher pressure. From these images, we observe two major changes as pressure increases. The first is that the flames at higher pressure exhibit more wrinkling. The Reynolds number proportional to pressure and so this result is not unexpected. It is also observed that the high-pressure cases exhibit more radial spread of the flame. A possible reason for the reduced spread is the decrease in laminar flame speed with increasing pressure. In fact, the laminar flame speed is computed to be about half its value at 1 atm. However, the increased wrinkling of the flame should lead to a higher turbulent flame speed, and so the laminar-flame-speed argument does not seem to be adequate. At this time, the reason for this difference is not entirely clear.

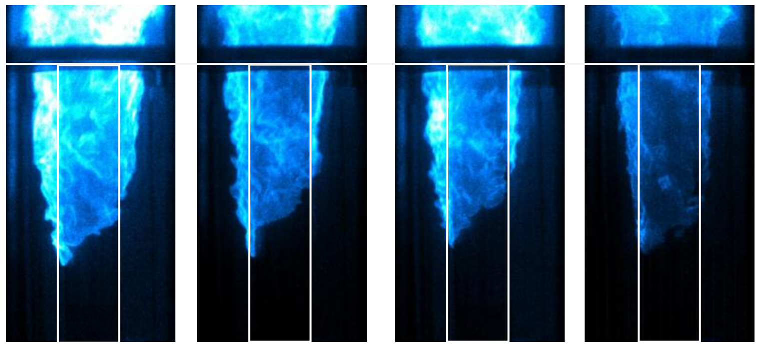

Figure 16. Chemiluminescence images of flashback at different pressures. Vertical and horizontal lines indicate the locations of center-body and the combustion chamber.

PIV during flashback was also conducted in the high-pressure chamber. Figure 17 shows PIV and luminosity results for flashback events at 1 atm and 5 atm. The bulk flow velocities in the two cases have been matched, and only the pressure is varied, which means the higher pressure case has a higher mass flow rate, and a factor of 5 higher Reynolds number. The images in Figure 17 were captured simultaneously at a framing rate of 5 kHz. The position of the PIV measurement plane in relation to the flame, which swirls into and out of the field of view during a flashback event, is shown in the form of a drawn-in green line in the synchronized chemiluminescence images. The luminescence images are taken from a perpendicular field of view. The direction of the flame is indicated by a blue arrow in Fig. 17, the direction of the approach flow by a red arrow. The flame front in the PIV results is marked by a red line. The contour plots show the axial velocity field. The white line marks an iso-velocity contour of 0 m/s. It is seen that at 5 atm the region of negative axial velocity upstream of the leading flame tip still exists, in agreement with the 1 atm case, which suggests the mechanism facilitating flashback is unchanged despite a factor of 5 higher pressure, and hence a factor of 5 higher Reynolds number.

Comparing the 5 atm case to the 1 atm case, it is seen that the radial flame spread differs significantly between the cases. It is known from the studies at 1 atm that the flame essentially pushes the approach flow out of the way (deflects the streamlines) due to the heat release. The decrease in radial flame spread with an increase in pressure may be explained by the higher momentum of the approach flow due to a higher density (as mentioned before the bulk flow velocity is kept constant). Hence, this confirms the picture that the flow acts against the incoming momentum through the heat release. A more detailed investigation of the results obtained at up to 5 atm is on-going.

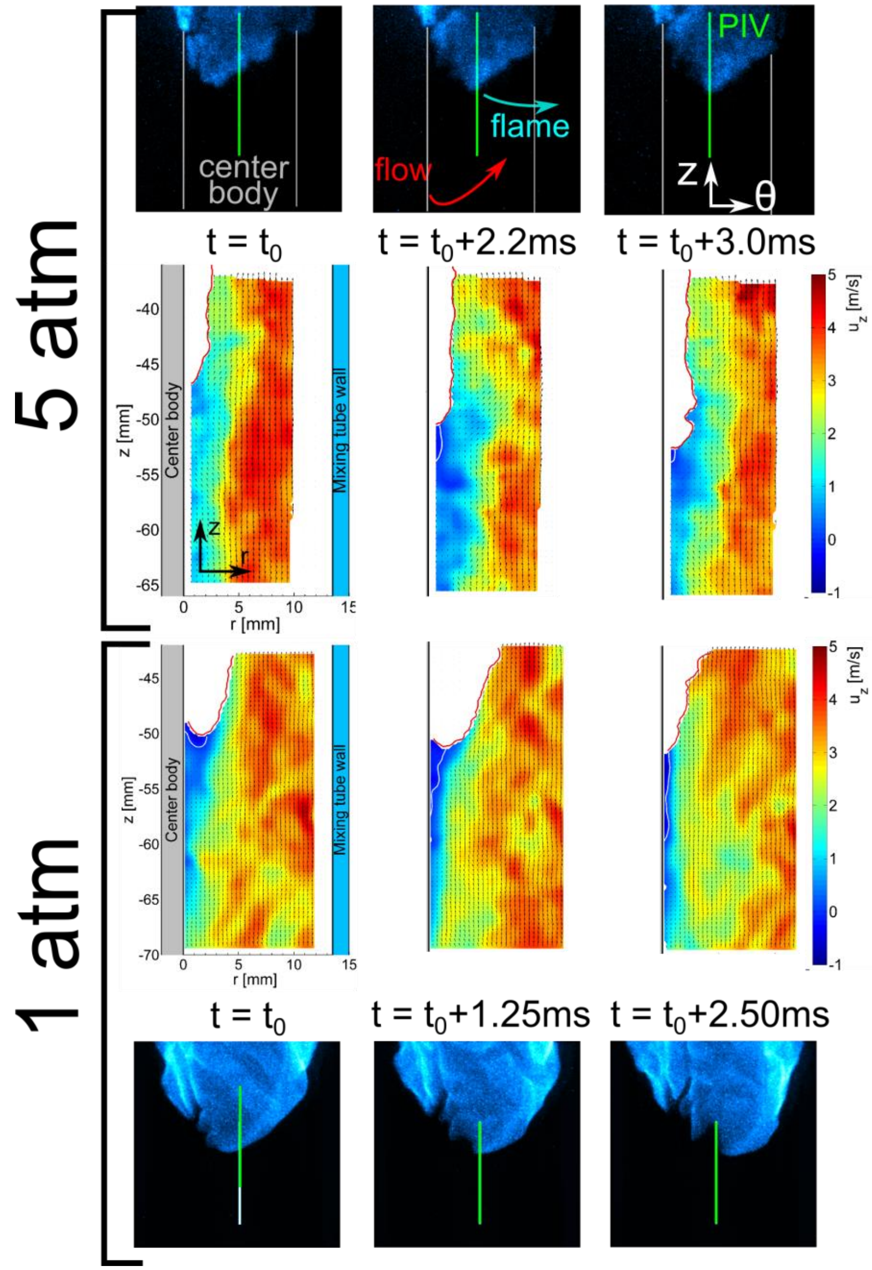

Figure 17. Velocity field results at 5 atm are compared to results at 1 atm. The position of the measurement plane in relation to the flame is shown in form of a green line in the chemiluminescence images, which are taken from a perpendicular field of view.

4.C Computational Program: Flashback in a canonical configuration

Boundary layer flashback introduces a new significant hurdle compared to other types of flashback. For instance, in the simulations of vortex breakdown based flashback it has been found that existing models reproduce flashback with reasonable accuracy, but unphysical near-wall flame propagation could be introduced by the nature of the chemical source term closures used (Tangermann & Pfitzner, 2009). The analysis is based on both *a priori* and *a posteriori* analysis of a direct numerical simulation (DNS) of channel flashback conducted by Gruber et al. (2012). The study assesses the key physical characteristics that need to be represented in order to repro- duce flashback using LES computations. Statistical quantities describing the structure of the flame front are proposed and used to evaluate LES performances.

4.C.1 DNS flow configuration

Figure 18 shows a schematic of the flow configuration used in both the DNS and LES computations. The domain measures 0.06 m × 0.012 m × 0.036 m in the streamwise, wall-normal, and spanwise directions, respectively. In the DNS computation, a 2400 × 480 × 1440 point computational grid is used. Premixed hydrogen-air mixture was fed through the inlet with a bulk velocity of 20 m/s leading to a Reynolds number of 3200. The equivalence ratio of the mixture was 0.55, and the inflow temperature was set at 750 K. Hydrogen combustion was simulated using a 9-species 19-step reaction mechanism (Li et al., 2004). Figure 19 shows instantaneous flame front contours at different times.

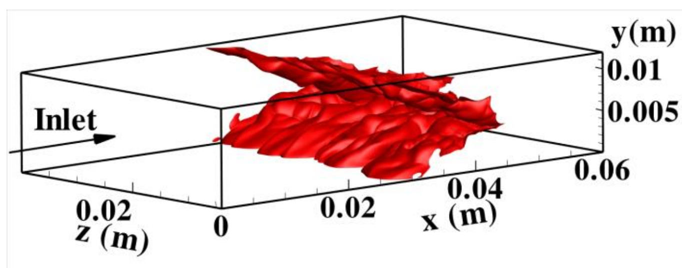

Figure 18. Channel flow configuration, where *x* is the streamwise direction, *y* is the wall-normal direction, and *z* is the spanwise direction. Shown in red is the DNS instantaneous iso-contour of progress variable c = 0.7 filtered with a Gaussian filter of size that is 8 times larger than the DNS grid size for t = 7.880×10^{-4} s, measured from the time of initialization.

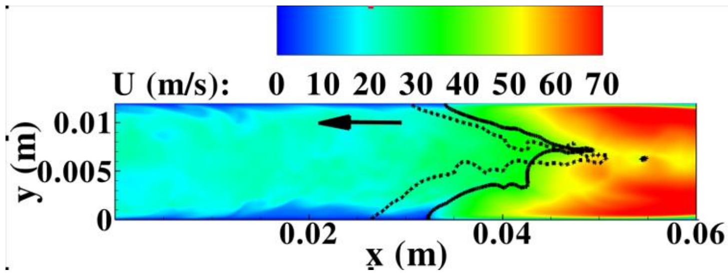

Figure 19. Instantaneous DNS contour of streamwise velocity component at t = 0.788 ms. The solid line represents the flame front isocontour based on c = 0.7 at that time instant, while the dashed line is the flame front at t = 1.44 ms. The arrow indicates the direction of flashback.

4.C.2 LES computations

The LES approach uses a grid-based filtering technique. The flame evolution is described using a flamelet approach, where a transport equation for the Favre-filtered progress variable is solved along with the filtered continuity and momentum equations.

$$\frac{\partial \bar{\rho}\widetilde{c}}{\partial t} + \nabla \cdot (\bar{\rho}\widetilde{\mathbf{u}}\widetilde{c}) = \nabla \cdot (\alpha(\widetilde{c}, \Delta_{LES})\bar{\rho} D \nabla \widetilde{c}) + \Im_c + \bar{\dot{\omega}} \qquad (1)$$

where α is a model for the correlation between the diffusivity and the scalar gradient, ΔLES is the LES filter width and $\dot{\omega}$ is the filtered chemical source term. The second term on the right hand side is the subfilter scalar flux term. In general, different models are available for closing these terms (Colin et al., 2000; Hernandez-Perez, 2011; Fiorina et al., 2010; Boger et al., 1998; Tabor & Weller, 2004). In this study, three different models were tested and are described Section 4.C.2. A low-Mach number technique based on a pressure-projection algorithm is used (Pierce & Moin, 2004; Akselvoll & Moin, 1996). The choice of a low-Mach number solver will be discussed in Sec. 4.C.4.

4.C.2.1 Progress variable based combustion models

All models implemented with this configuration use the progress variable *c* approach introduced in Sec. 4.C.2. The evolution of the flame is described by solving for the progress variable. In this work, the progress variable is defined as

$$c = \frac{Y_{H_2} - Y_{H_2,u}}{Y_{H_2,b} - Y_{H_2,u}}$$

where Y_{H_2} is the local mass fraction of H_2, $Y_{H_2,u}$ is the mass fraction of H_2 is the fresh gases and $Y_{H_2,b}$ is the mass fraction of H_2 is the burnt gases (close to zero for a lean mixture).

Direct flamelet model

In the Direct Flamelet (DF) model, the 1-D laminar premixed solution is directly mapped to filtered progress variable space, and no convolution rules are used to transform the raw progress variable to a filtered value. All unclosed terms are determined by first computing a mapping between the progress variable chosen and the terms needed to be mapped. To compute this mapping, a steady 1D laminar premixed flamelet simulation with detailed chemistry is performed using the Flamemaster code (Pitsch).

Filtered tabulated chemistry for LES (F-TACLES)

In the Filtered Tabulated Chemistry for LES (F-TACLES) approach, the 1D laminar flame solution is filtered using an explicit Gaussian filter, which is different from the LES filter. As described by Auzillon et al. (2011), the three terms on the right hand side of Eq. 1 can be directly obtained from this filtering procedure. This model artificially thickens the flame when constructing the filtered mapping variable by filtering the 1D flamelet solution with a filter width larger than the LES filter width.

Algebraic flame surface density model (AFSD)

The AFSD model is based on a flame surface density approach, and does not explicitly rely on the flamelet assumption. The flame surface density is obtained with an algebraic model Boger et al. (1998) that relates the subfilter variance of progress variable to the flame surface density.

$$\Sigma = 4\beta\frac{\overline{c}(1-\overline{c})}{\Delta}$$

with β being a tunable coefficient and Δ the LES filter width.

4.C.2.2 Heat loss modeling

Parameterize heat losses

Given a set of boundary conditions for the mixture composition and thermodynamic properties, a steady 1D adiabatic freely propagating premixed flame simulation can give Y = Y(C). In the context of boundary layer flashback, the flame is also expected to strongly interact with the cold walls. In the case of boundary layer flashback the vector normal to the flame front near the wall is supposed to be aligned with the wall.

Under this assumption, the flame is expected to exchange heat with the wall while reactants are being consumed. It is then natural to parameterize the heat loss dimension with a sink term for the temperature transport equation in the 1D simulations, rather than by changing temperature or mass flow rate boundary conditions (Trisjono et al., 2014; Mercier et al., 2014; Menon et al., 2013). The form of the sink term also depends on the nature of heat losses. In the present case, a temperature sink term is used, similar to Hergart and Peters (2002), namely,

$$\dot{Q} = \frac{\lambda(x)(T(x) - T_w)}{q^2}$$

where *T(x)* is the gas temperature, T_W is the wall temperature and λ(x) is the heat conductivity. For this case, the wall temperature is held constant at 750K, *q* parameterizes the strength of the enthalpy loss and can be interpreted as the distance from the wall. The smaller value that *q* takes on, the higher the amount of heat that is exchanged with the walls.

For the actual chemistry tabulation, the variation of *q* is considered embedded in the variation of the total enthalpy H_{tot} of the gas (formation+sensible). The underlying assumption is that for a given C value, H_{tot} is only parameterized by *q*. To simplify boundary conditions, the tabulation is actually expressed in terms of enthalpy defect H defined by $H = H_{tot} - H_{tot,adiabatic}$, similar to Mueller & Pitsch (2012)

Covered enthalpy range and extrapolation

Because the enthalpy sink used to represent heat losses is proportional to temperature, it is mainly active in regions where hot gases are present (C close to 1). For C = 1, the enthalpy defect range covered is then larger than for C = 0.5 as it can be seen on Figure 20.

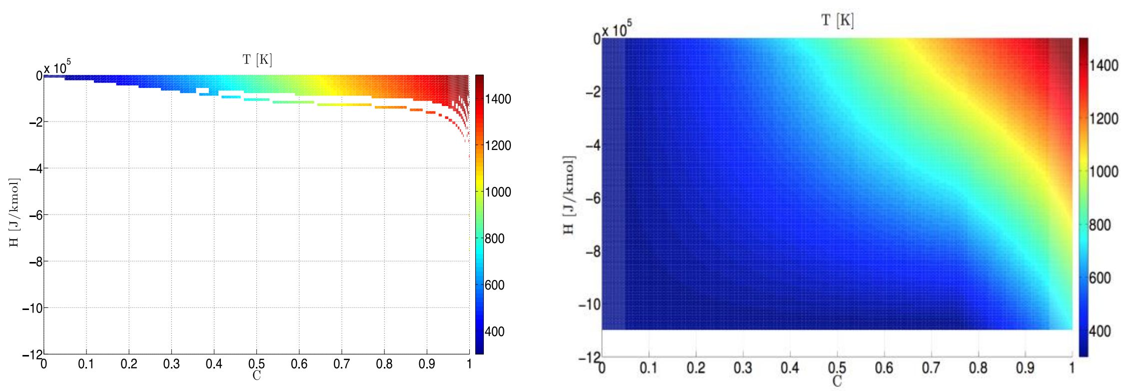

Figure 20. Incomplete (C,H) mapping (left), Extrapolated (C,H) mapping (right)

The (C, H) space represented on Figure 20 is however only a region where the flame can sustain (the eigenvalue problem solved by the steady 1D adiabatic freely propagating premixed flame code has a solution). At a fixed C, lower total enthalpies can potentially be encountered if the reaction has stopped but the flow still loses heat. To cover this region not represented by the reacting code, a frozen chemistry assumption is used and based on the lowest enthalpy represented by the reacting code. More specifically, for a fixed C, it is assumed that as the total enthalpy decreases, the formation enthalpy remains identical and only the sensible enthalpy is affected. The change in total enthalpy can then directly be mapped to a change in temperature as illustrated on Figure 20.

Using scaling properties described in (Trisjono et al., 2014) all the other variables can then be deduced from their value at the closest point given by the reacting 1D code in the total enthalpy space, and the temperature variation with the point where the variable needs to be extrapolated.

4.C.2.3 Preferential diffusion

The fuel mixture simulated in this case contains large amounts of hydrogen burning in a low Reynolds number flow. Preferential diffusion may then play a non-negligible role in the flame propagation. In the steady 1D adiabatic freely propagating premixed flame simulations, Schmidt numbers and Lewis numbers are different from 1, using the Curtiss-Hirschfelder approximation (Curtiss & Hirschfelder, 1949). Similar to de Swart et al. (2010) and Mercier et al. (2014), preferential diffusion is included in the tabulated chemistry by adjusting the diffusivity of C with the known diffusivities of the species defining C. It is then crucial to include species which Lewis number departs the most from 1 in the progress variable definition.

4.C.3 LES Results

Two different groups of LES calculations are carried out. First, the effect of the combustion models is tested using the three models described in Sec. 4.C.2.1. Second, the effect of filter width is discussed.

4.C.3.1 Quantitative parameters

To understand the LES results, two quantitative parameters are introduced to describe the macroscopic flame structure and the flame propagation. The evolution of the distance between the leading and trailing edges of the flame is studied. This quantity, termed as flame depth here, incorporates the cumulative effect of the core velocity on the propagation characteristics.

Figure 21 shows the spanwise averaged depth as a function of time. It is seen that for the baseline case (red line) this quantity increases with time but ultimately reaches a slowly varying stage after 0.5 ms. The depth in the DNS is steady in this time interval at roughly 0.015 m. The F-TACLES flame is the only solution that also seems to reach a slowly varying stationary state.

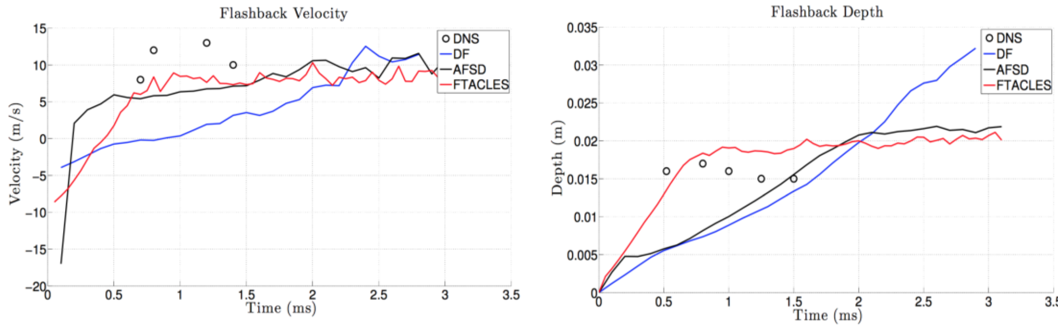

Figure 21 Spanwise averaged depth parameter (left) and flashback speed parameter (right) as a function of time for DNS (circles) and LES with F-TACLES (solid line), FSD with β = 0.2 (dash-dotted line), and FSD with β = 0.66 (dashed line) at $\Delta_{LES} = 8\Delta_{x,DNS}$.

To analyze the flame propagation, a second quantitative parameter denoted as flashback velocity is introduced. This parameter is computed based on the evolution of the volume of burnt mixture in the domain. This is a global parameter that does not take into account the difference between walls and core flow.

Figure 21 shows the flashback velocity variation in time for the models considered in this study. It can be seen that initially the flame is convected downstream (negative velocity) before flashback takes hold. But even then, the propagation velocity is lower than the DNS velocity.

4.C.3.2 Effect of combustion model on flame propagation

To understand the role of the model in predicting the parameters of flashback defined in Sec. 4.C.3.1, the three different models described in Sec. 4.C.2.1 were used with $\Delta_x = 8\Delta_{x,DNS}$. The DF model produced very inaccurate results. It was in fact found that the flame propagation was very dependent on the scheme used for the scalar interpolation. The results for DF are shown in this section to emphasize the role of the resolution of the filtered flame front.

The F-TACLES model is accurate in representing flame propagation. Quantitatively, the depth parameter (Fig. 21) is accurately represented. However, it can be seen that the flame wrinkling is clearly underestimated compared to the DNS data. The post-flame velocities are of the same order as in the DNS. It can be also observed that the blockage effect induced by the flame (V-shape acceleration of the flow field) is underestimated compared to DNS.

The AFSD model fails to represent the mean flame shape. This is very likely due to the fact that diffusion is taken into account in the flame normal direction, but does not depend on the flame topology. The flame shape follows directly the velocity profile in the channel. As the flame stretches with time, the DNS- based flashback velocity parameter gradually increases to nearly the value found from the F-TACLES model (Fig. 21).

4.C.3.3 Effect of LES grid on propagation

Three different grid sizes of 4, 8, and 16 times the DNS grid spacing were used. For all these computations, the F-TACLES model was used with a constant flamelet filter size $\Delta_F = 25\Delta_{x,DNS}$. In addition, the computational grid associated with each width was refined in the wall-normal direction to add twice the number of points in the low-velocity region. Grid clustering did not change the propagation speed or the depth parameter as compared to the uniform mesh case for both filter widths. This was surprising, as better near-wall resolution should be expected to better represent the flashback process. This suggests that a minimum resolution is needed to reproduce flashback but additional resolution does not necessarily introduce any new physics capable of altering the flame dynamics. However, the change of filter width from $8\Delta_{x,DNS}$ to $16\Delta_{x,DNS}$ had a large effect on the transient flame evolution. Figure 22 shows the evolution of the depth parameter for the three filter widths. It can be seen that not much difference can be observed between $4\Delta_{x,DNS}$ to $8\Delta_{x,DNS}$. For the coarsest mesh, the transient evolution of the flame depth is not accurately represented. However, the flame reaches a final flame depth close from the other reached by the finer simulations.

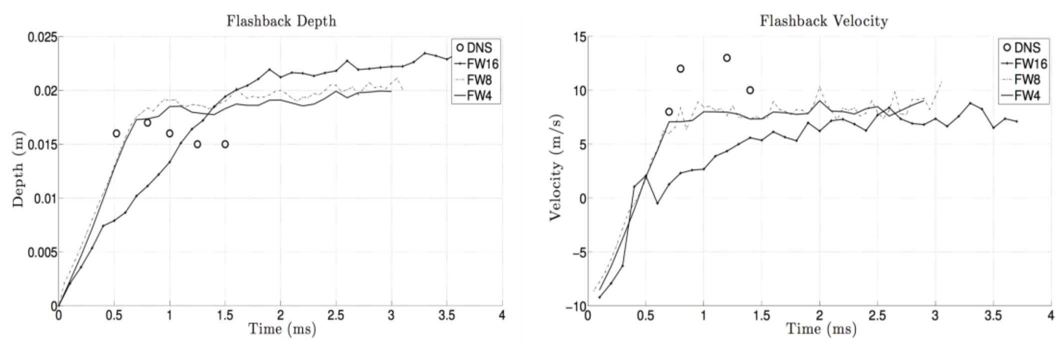

Figure 22. Plot of spanwise averaged depth parameter (left) and flashback speed parameter (right) as a function of time for DNS (circles) and LES with F-TACLES with $\Delta_{LES} = 4\Delta_{x,DNS}$ (solid line), $\Delta_{LES} = 8\Delta_{x,DNS}$ (dashed line) and $\Delta_{LES} = 16\Delta_{x,DNS}$ (solid line with dots).

4.C.4 The effect of compressibility on flashback

Despite representing additional physical processes in the simulation of boundary layer flashback, such as heat losses, it was observed that the flashback speed was underestimated compared to DNS and experiments. The LES carried out always assumed a low- Mach number flow regime in the combustor. DNS results including compressibility effects obtained by Gruber et al. (2012) led to the conclusion that the expansion process could be critical in triggering flashback and enhancing the flame acceleration. The influence of the compressible assumption on the simulation of boundary layer flashback was therefore investigated. Impacts on small-scale and large-scale-features are described.

4.C.4.1 A priori description of the numerical compressibility

In this comparison between the low-Mach and the compressible solver, a flamelet-progress-variable combustion model was used. Although a similar combustion model is used, the low-Mach and the compressible solver will inherently differ in terms of the physical representation of the combustion process. The low- Mach number directly maps the flame motion to density variation. This is in turn leads to velocity changes coupled with pressure gradients variations in order to ensure mass conservation. It eventually affects the flame motions. The combustion process in the compressible solver is somewhat reversed. The flame motions affect the heat transport equation, which is coupled to the pressure gradients through thermodynamics. Only then, the velocity is affected by the pressure gradients, and the density varies in order to conserve mass. The two main differences that can be highlighted are first that pressure and density switched roles. In the low-Mach number solver, the density carries the information of the flame motion and the pressure purpose is to ensure mass conservation. In the compressible solver, the pressure gradients carry the information of the flame motion and the density eventually ensures mass conservation. Second, the propagation of information of the flame motion is instantaneous in the low-Mach solver. In the compressible solver, the pressure jumps have to propagate at a finite speed (speed of sound). Presumably, the second point can turn out to be important in the study of transient effects such as boundary layer flashback.

4.C.4.2 A priori effect of compressibility

A crude description of compressibility in the flashback problem can be provided in terms of the Ma number. Conventionally, for Ma numbers lower than 0.3, compressibility effects are neglected. As seen in Figure 18, we fall in this regime in the flashback problem.

Another conventional description of the compressibility can be formulated in terms of the effect of the pressure on the density field. The density field can be affected by composition and temperature changes due to the combustion, and by fluctuating pressure variations. The former impact on density field can be cast

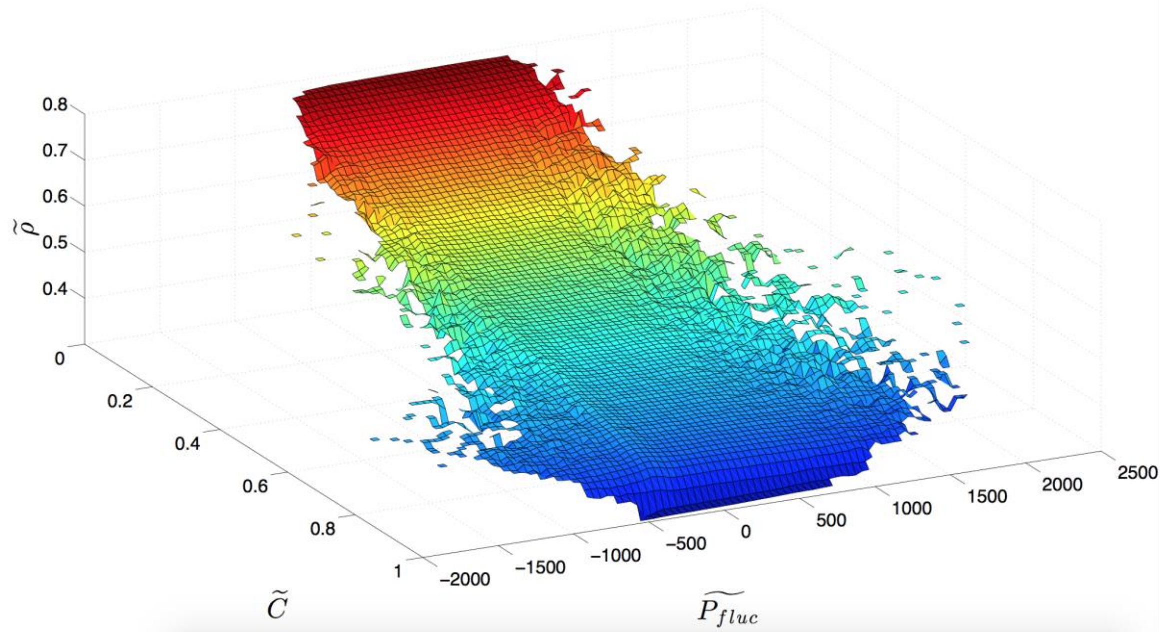

Figure 23. Representation of the common impact of pressure variation and combustion on the density field From this analysis it can be seen that the effect of compressibility is weak with regards to the usual description of compressibility effects.

in terms of the progress variable changes, viz.,

$$d\rho = \frac{\partial \rho}{\partial C} dC + \frac{\partial \rho}{\partial P} dP$$

The latter part can be cast in terms of the fluctuating pressure. Note that for the compressible solver, this latter part has an effect on density whereas this is neglected for the low-Mach number solver. Figure 23 illustrates these competing effects.

4.C.4.3 Effect of compressibility on the flow expansion

As it can be seen in Figure 24, the density field follows a different profile when using a compressible solver compared to a low-Mach number solver, where density is prescribed by a 1D incompressible flamelet equation. In particular, it can be observed that the density variations are steeper for the lowest values of progress variable in the compressible solver compared to the low-Mach number solver. This can increase the blockage effect of the flame, deviating further the streamlines to the core of the flow, and increasing the strength of reverse flow pockets in front of the flame (Fig. 25).

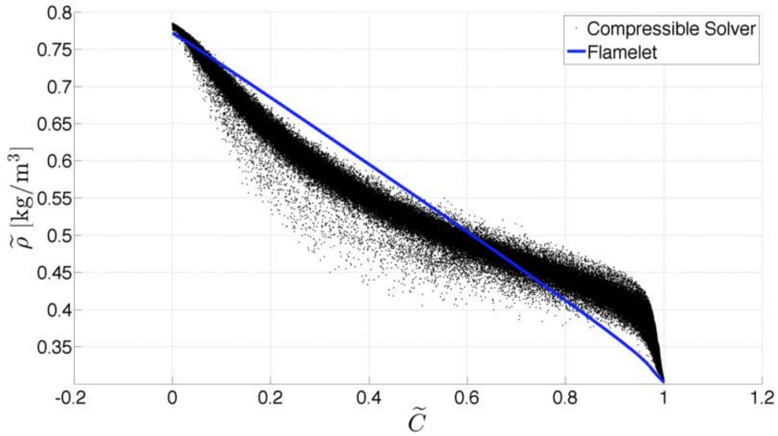

Figure 24. Density field evolution with progress variable in the compressible solver and the low-Mach number solver.

4.C.4.4 Effect of compressibility on quantities of interest

The main quantity of interest in this problem the flashback speed, which is represented on Figure 12. The compressible solver does not substantially change the prediction of the flashback speed. The transient evolution of the flame is however observed to differ in both cases. In the compressible solver, the flame acceleration stops earlier than in the low-Mach number solver (phase 1 on Figure 26).

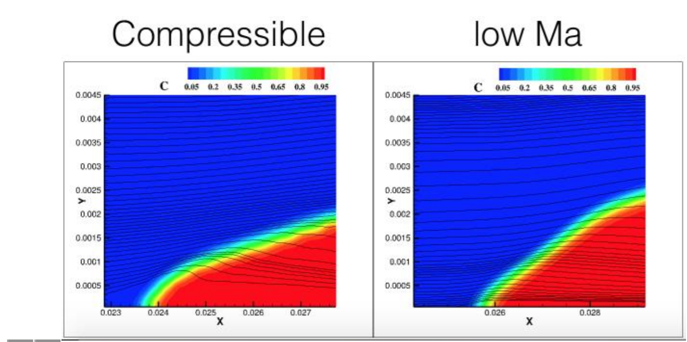

Figure 25. Impact of compressibility of flame blockage effect and the formation of backflow pockets.

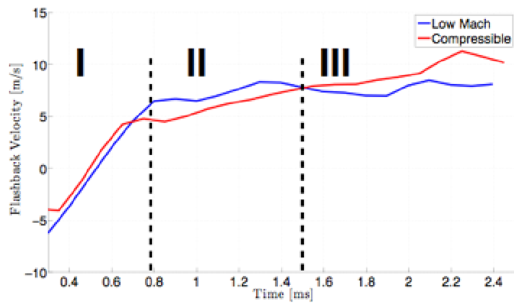

Figure 26. Flashback speed in the compressible and low-Mach number solver.

It could be seen than this was due to a delay in the development of flame wrinkling for the compressible solver. In the low Mach number solver, it mainly takes place at the end of phase 1. The flashback speed in the compressible solver keeps increasing in phase 2 while it remains stable for the low-Mach number solver. It was observed that during this phase, the flame depth kept on increasing for the compressible solver. At the end of phase 2, the flashback speed keeps on increasing but the flame depth of the compressible solver stops increasing. The flame starts in fact to get wrinkled.

4.D Computational Program: Effect of fuel stratification on turbulent flame propagation

Fuel stratification is a physical phenomenon that has very high significance in both stationary and aircraft gas turbines, albeit for different reasons. In combustors for power generation, the fuel is premixed with compressed air and injected into the main combustion zone. Ideally, this high temperature flame is confined to a prescribed portion of the combustor. However, due to operational variations, there is a likelihood that the flame will propagate upstream of the combustion zone into the premixed section, which is not designed to hold high temperature gases and will thus lead to device failure. In combustors that use high hydrogen content fuels, this flashback occurs through flame propagation in the boundary layers. One strategy for arresting this flame flashback is through fuel stratification in the premixing zone, where lower fuel mass fraction is injected near the boundary layers which augments near-wall flame quenching.

Based on this discussion, the objective here is to understand the structure of a turbulent premixed flame propagating through variable equivalence ratio mixtures. For this purpose, a homogeneous isotropic turbulence with uniform mean flow is considered. Direct numerical simulation of this configuration using detailed chemical kinetics is carried out for hydrogen/air combustion. Equivalence ratio fluctuations are introduced in two different ways to study the impact of the length scales of fluctuations on the flame front evolution.

4.D.1 Simulation configuration

The effect of fuel stratification on flame propagation is studied using DNS with detailed chemical mechanism. The DNS cases studied use a computational domain that is periodic in the y and z directions, and has an inflow and outflow in the x direction (streamwise direction). The computational domain spans 0.5h×h×h in the stream-wise, stream-normal and span-wise directions, where h = 4cm. The flame front location is controlled using a closed-loop feedback algorithm (Appendix) that adjusts the inflow velocity such that the flame is contained within a short region in the streamwise direction. Hence, the streamwise length is shorter compared to the other two directions. The computational grid 256 × 512 × 512 in the three directions, respectively. Figure 27 shows the dimensions of the computational domain.

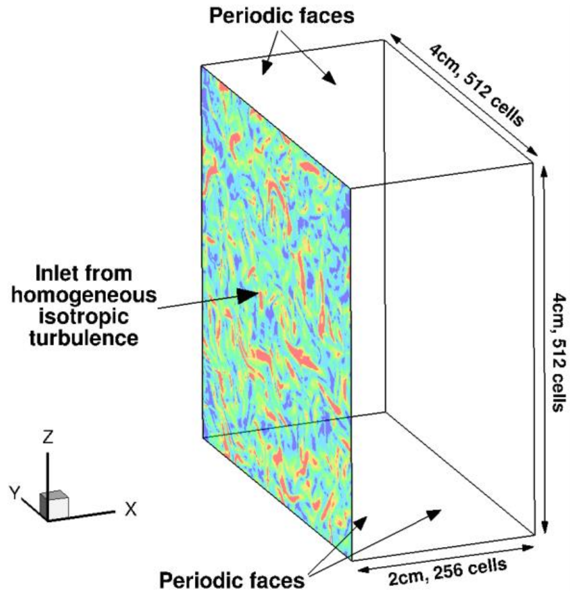

Figure 27. Sketch of the computational domain, with instantaneous vorticity plotted on the inlet plane. Inlet condition is from a homogeneous isotropic turbulence DNS.

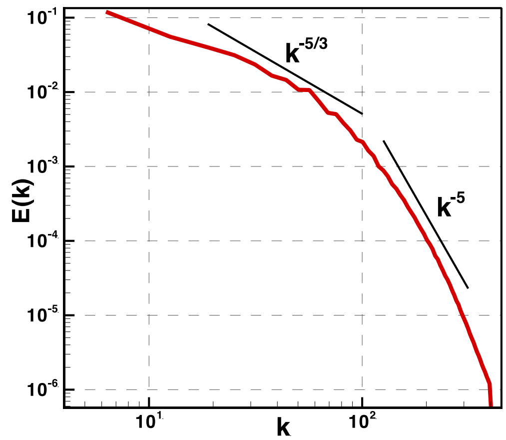

Figure 28. Spectrum of HIT DNS for inflow velocity boundary condition generation.

The inflow boundary conditions require more description. Macroscopically, a mean flow velocity that is roughly $2.3S_l$, where S_l is the laminar flame speed at stoichiometric conditions, is imposed. To generate time and space correlated structures at the inflow, a separate homogeneous isotropic turbulence (HIT) is used. A linear forcing is imposed (Lundgren, 2003; Rosales & Meneveau, 2005) until the turbulence is in a statistically stationary state. The kinetic energy spectrum corresponding to this HIT is given in Fig. 28.

Two different cases with stratification were studied, named large-scale stratification (LSS) and small-scale stratification (SSS). For both these cases, the inflow turbulent field fed to the main flame simulation is identical, but the difference lies in the introduction of the scalar field. The objective of these studies is to introduce equivalence ratio fluctuations such that the flame front experiences time-evolving fuel-to-air ratios. In the case of the LSS, the fuel-air ratio is introduced as a uniform value in the inlet plane but changes in time from an initial value of 2 to 0 over 1ms, which is roughly equivalent to 3/4 of a flow-through time. In the SSS case, a spectrum of length scales is used to generate a three-dimensional scalar field of mixture fraction, which is then fed to the inlet plane of the flame simulation. The scalar field is generated in a similar manner to Eswaran and Pope (1988). Without reaction, the scalar evolves in the domain as depicted in Fig. 29.

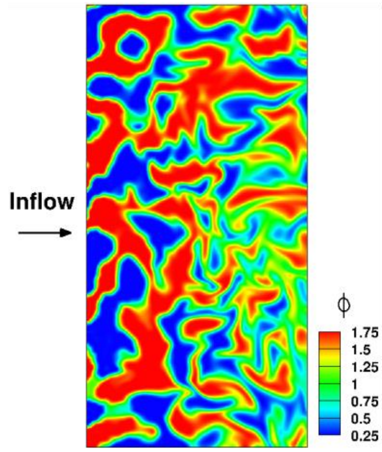

Figure 29. A decaying passive scalar field transported using a turbulent flow field in the streamwise direction.

4.D.2 LES Results

4.D.2.1 Large-scale stratification (LSS)

The LSS case involves large-scale variation of the equivalence ratio. Due to the nature of the flow, these variations do not cascade down to the small scales in the distance between the inlet and the flame, and retain much of their large-scale features. Figure 30 shows the evolution of the flame front with time. The domain is initialized with an equivalence ratio of 2, which is progressively replaced by lower values as the inflow conditions change with time. As the equivalence ratio seen by the flame initially moves towards stoichiometric condition, the flame is seen to become thinner, with increased source terms and peak temperatures. Note that resolution of the DNS is chosen such that the grid adequately captures the thinnest flame zone. As the equivalence ratio further drops, the flame front becomes broader with lower temperatures across the front. The post-flame temperature is also lower indicating increased dilution of heat release. Beyond the lower flammability limit, the flame extinguishes as expected.

Figure 31 shows the evolution of the flame surface corresponding to a temperature of 1000K. In the initial phase of the simulation, the strong combustion leads to heat-release generated small-scale structure that causes extensive flame wrinkling. It is also seen that the post-flame velocities can reach velocities up to three times the inflow velocity, corresponding to gas expansion from heat release. This strong streamwise gradient in velocity generates the vortex structures that case flame wrinkling. As the equivalence ratio decreases, heat release is also reduced, which affects the post-flame velocities. As seen in Fig. 31, at later time, the post-flame velocities do not increase substantially beyond the inflow velocities. Consequently, flame wrinkling is also reduced leading to lower equivalent turbulent burning velocity. It is important to note that this reduction in surface area further decelerates the flame, pushing the system towards extinction.

Figure 30 also shows the comparison in composition space between the DNS and premixed flamelet calculations. The flamelet solutions were obtained at different equivalence ratios for a one-dimensional system with identical chemistry mechanism. Interestingly, the scatter plot in composition space follows closely the flamelet solution. At different times, the flame front experiences different equivalence ratios, which is reflected in the composition space plot where the scatter aligns with different premixed flamelet solutions.

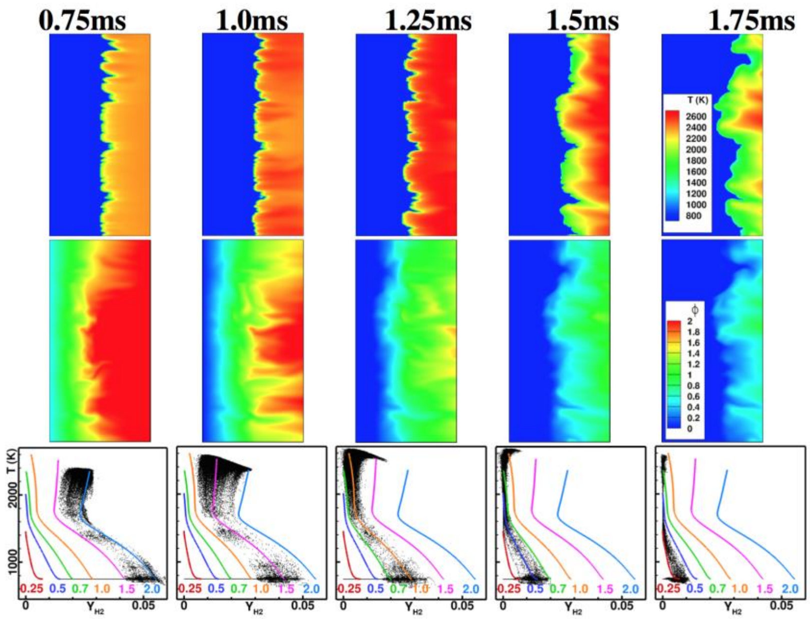

Figure 30. (Top) Temperature and (middle) ϕ and (bottom) composition space plots at different times from the initial condition. Several flamelet solutions for different ϕ's between 0.25 and 2 are plotted on top of the composition space plots. Inflow ϕ varies between 0ms and 1ms, from 2 to 0.

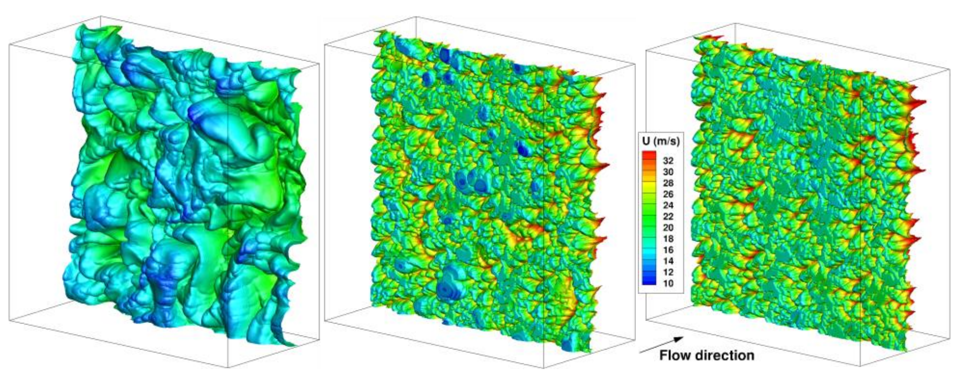

Figure 31. Isosurface of temperature (1000K) colored by the local streamwise velocity, corresponding to the first, third, and fifth timeframe in Fig. 30.

This confirms the notion that large-scale equivalence ratio variations could be seen as merely a collection of propagating premixed flames at different equivalence ratios. In this sense, the structure of the flame is not affected by stratification.

4.D.2.2 Small scale stratification (SSS)

The SSS case presents a different scenario, where the integral length scale of the scalar structures is roughly 10 times the grid spacing. Here, the equivalence ratio fluctuations occur at scales comparable to the flame thickness, which implies that strong variations could occur where the chain branching reactions take place. Note that this flame is statistically stationary as opposed to the LSS case that is time evolving due to the changes in the inflow conditions. Figure 18 shows the temperature, equivalence ratio, and streamwise velocity fields in a two-dimensional plane at the center of the spanwise direction. It is seen that the flow retains the small-scale variations in equivalence ratio as it encounters the flame. The flame front is more complex than that for the LSS case, with regions of very low temperature corresponding to the presence of low equivalence ratio fuel/air mixture. Since the length scale of these structures is comparable to the flame thickness, low temperature streaks are found to penetrate deeper in the streamwise direction.

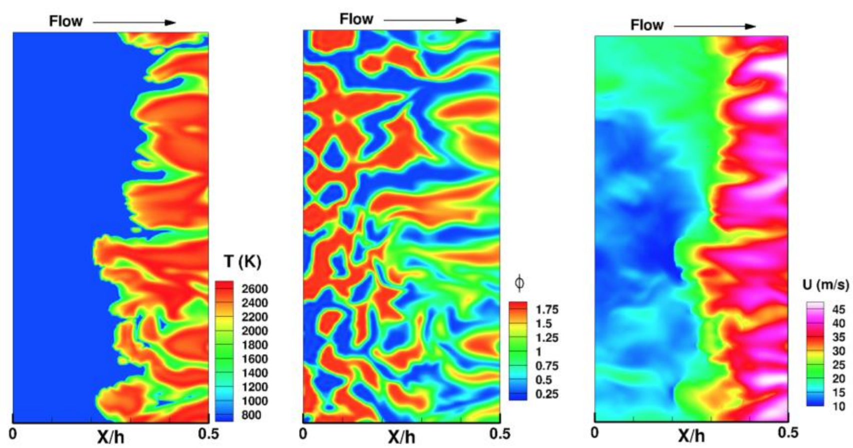

Figure 32. Instantaneous temperature, equivalence ratio, and streamwise velocity plotted at the center plane in the spanwise direction.

Figure 33 shows the isocontours of temperature for the SSS case. Compared to the same plot for the LSS case (Fig. 31), the SSS case shows larger structures. This is mainly due to the low or high equivalence ratio regions that have reduced heat release compared to stoichiometric mixture. This reduces the gas expansion and the post-flame velocity and the velocity gradients across the flame, which reduces flame wrinkling. The presence of the small-scale structures distinctly changes flame evolution. If the equivalence ratio falls below the flammability limit, this will introduce flame holes that will propagate and mix with the burnt gases post-flame. If this mixing happens with higher than stoichiometric but burnt regions, a secondary flame zone could be formed. Hence, such intense stratification is fundamentally different from the LSS case.

Figure 34 shows the composition space plot similar to that for the LSS. It is seen that the flame front now spans a number of different flamelets, with the flame front found at a number of different equivalence ratios. The composition plot itself does not describe the structure of the flame, which shows structures that are not typically observed in premixed flames (Fig. 33).

4.E Computational Program: Implementation of the computational tool in a realistic configuration

4.E.1 Configuration

An experimental swirl burner (UT Swirler) was designed to replicate the premixing chamber in modern gas turbines. The burner consists of two sections: a toroidal mixing tube and a combustion chamber. Far upstream near the inflow plane, eight vanes are evenly spaced around the central body. The air and fuel are premixed upstream before passing through a flow straightener and entering the mixing tube through the inlet. This allows the flashback to proceed in fully premixed mode, rather than through a stratified mixture. The expansion causes vortex breakdown, yielding a low velocity core, which holds the conical flame in the stable case.

The configuration used can therefore reasonably emulate burners used in the industrial context. However, they are numerically challenging since they require low energy dissipation so the core and precessing vortex associated with the swirl can realistically affect the flame front.

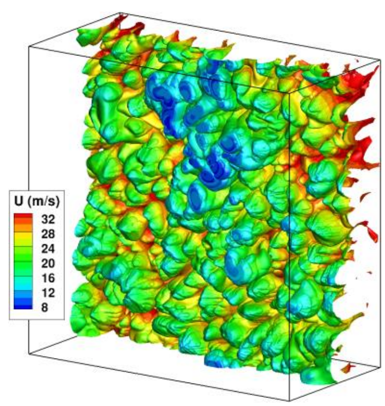

Figure 33. Isosurfaces of temperature (1000K) colored by the local streamwise velocity.

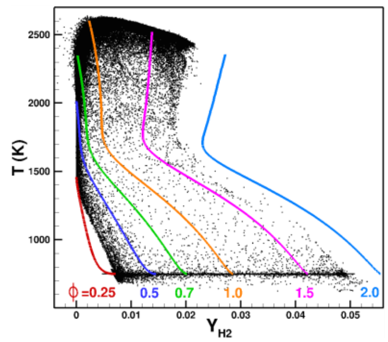

Figure 34. **Conditional plot from SSS compared to flamelet solutions for different equivalence ratios.**

The chosen numerical procedure has been implemented in OpenFOAM in order to ease the interaction with external users.

4.E.2 Solver design

4.E.2.1 Low-Mach number procedure

The solver developed uses the low-Mach number assumption and solves the pressure field using a projection procedure of the velocity field onto a mass conservative space. The solver is specifically designed to use flamelet models but other combustion models can also be easily implemented. The coupling between the scalars and velocity fields is ensured through outer iterations. The pressure projection algorithm uses the PISO procedure (Issa, 1985) classically used in OpenFOAM.

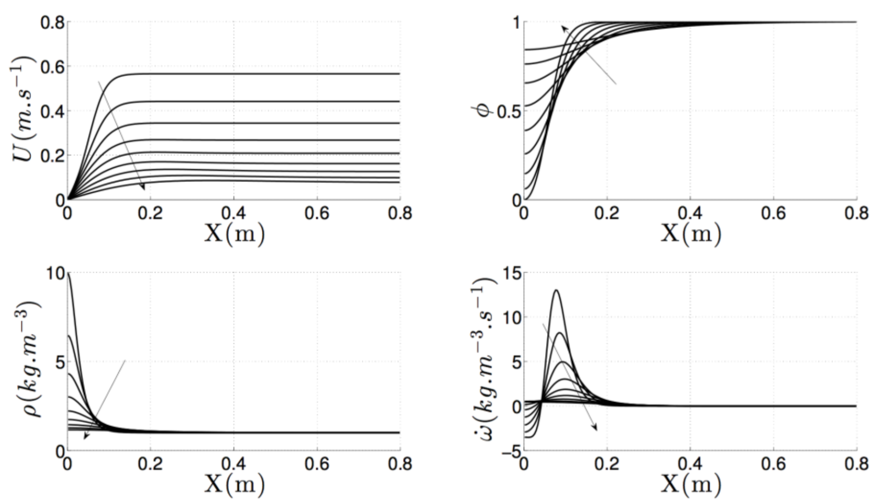

Figure 35. Analytical solutions of the 1D MMS problem. The arrows point in the direction of increasing time from 0 to 1s.

No low-Mach solver had been previously implemented *per se* in OpenFOAM and compressible solvers were usually used to handle variable density problems. The new solver was properly validated using the method of manufactured solution (MMS). The case used is a 1D mass diffusion through scalar diffusion and is illustrated on Fig. 35 (Shunn et al., 2012).

It can be seen on Fig. 36 that the solver gives 2nd order time convergence for the scalar field for large time steps and then 1st order for smaller time steps. This is expected since for small time steps, the spacing convergence takes over on the time convergence. More importantly, it can be seen that the new solver gives more accurate results than the compressible solver available in OpenFOAM. In fact mass conservation was not strictly enforced in OpenFOAM and gradually increased the error on the transported field (Fig. 23)

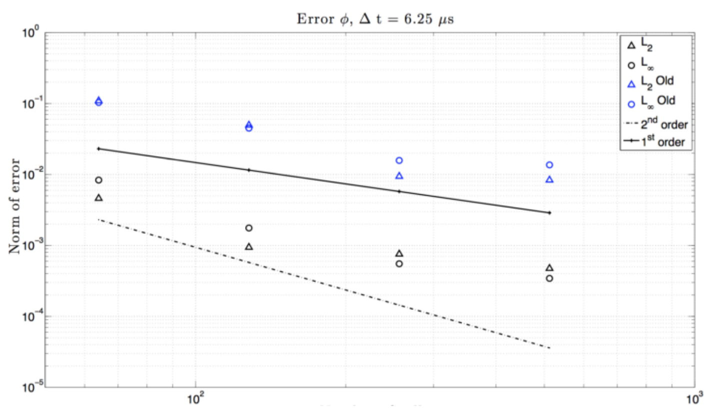

Figure 36. Error convergence of the scalar field computed between the solver output and the analytical values.

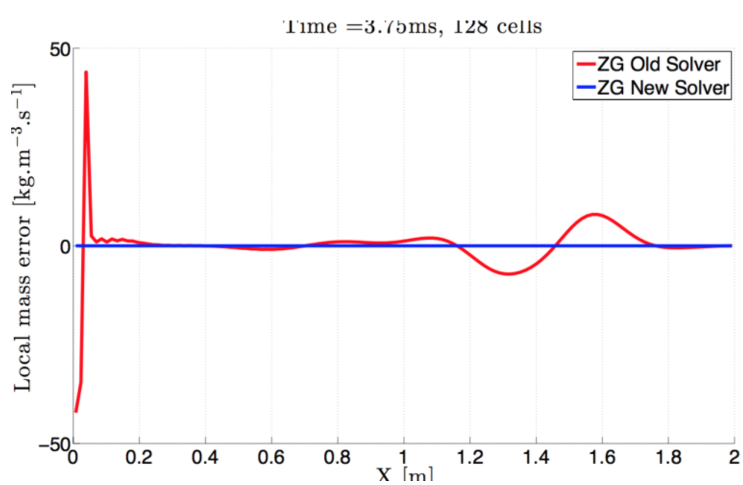

Figure 37. Local mass conservation error comparison between the OpenFOAM compressible solver and the newly written solver.

4.E.2.2 Kinetic energy conservation

Regarding the specific application considered, the solver has to be optimized to dissipate as little turbulent structures as possible. To do so, the numerical schemes are chosen so the solver does not dissipate kinetic energy.

The energy-conservation strategy is based on the scheme proposed by Morinishi (2010). This scheme reduces to the approach of Ham and Iaccarino (2004) in the limit of constant density flows. For a uniform mesh, the linear interpolation reduces to a mid-point interpolation scheme that minimizes an energy loss (Felten & Lund, 2006). The mid-point interpolation is also applied in the time direction, where the momentum transport equations are evolved from time n to n + 1, while the individual terms in the equation are evaluated at time n + 1/2 obtained using interpolation method. This implicit formulation is crucial for the conservation of kinetic energy. In other words, ensuring convergence of the time discretization is important to minimizing discrete energy loss. In the OpenFOAM solver, this is ensured using PISO (pressure-implicit second order) iterations (Issa, 1985). It has been shown that two PISO iterations are sufficient to achieve second order convergence in time (Issa, 1985). Note that this strategy is targeted towards statistically stationary flow problems. For a more general tool, fractional time-step procedure can be utilized (Kravchenko & Moin, 1997). To demonstrate the energy conservation properties of this solver, verification studies using canonical flow configurations were considered (similar to that in Mahesh et al., 2004). A Taylor-Green vortex with no density change was computed on orthogonal and skewed meshes. Figure 1 shows the solution on these two grids at the same computed time. It can be seen that the solver preserves the vortical structures even in a skewed mesh representation, which is important for application to complex geometries. Figure 38 shows the decay of kinetic energy for this test case. Not only the implemented approach is unaffected by mesh skewness, it shows comparable amounts of energy loss to the Ham and Iaccarino (2004).

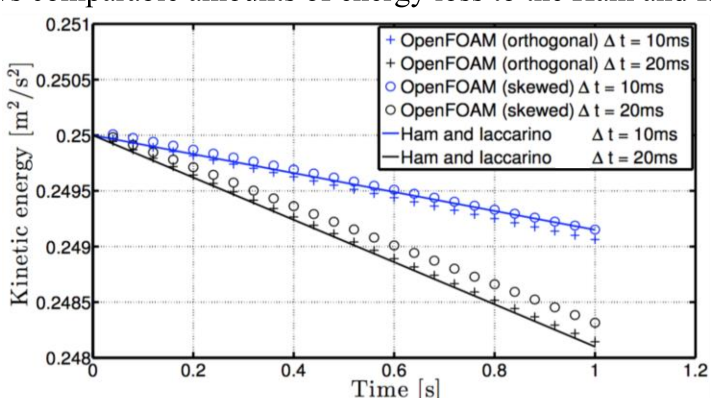

Figure 38. Temporal kinetic energy decay between different numerical approaches for orthogonal and skewed meshes, for two different time step sizes. Ham and Iaccarino (2004) results (solid lines) correspond to both orthogonal and skewed mesh cases.

4.E.3 UT swirl combustor simulation

The primary motivation is the study of flashback, quantified predominantly through the flashback speed. In order to isolate the effects of the model, the flow field is first examined in the absence of combustion and compared against the corresponding experimental data acquired in the current study. Qualitative and quantitative examinations of the stable reacting case and mixing tube flashback follow.

4.E.4 Inert flow structure and validation

Figure 39 shows radial plots of the streamwise and azimuthal components of velocity averaged in time and the azimuthal spatial coordinate. Near the combustion chamber (e.g. blue plane), both simulation components compare favorably with the experimental results. Discrepancies between the data sets grow as upstream slices are considered, though they remain within a single standard deviation in all but the last case (green plane). In particular, the experimental streamwise component is increasingly over-predicted. RMS velocities were found sensitive to the mesh resolution on near the vanes. A good agreement could be obtained with 12M cell mesh as illustrated on Figure 40.

4.E.5 Reacting flow: stable flame and flashback

To gain a general idea of the flame behavior as it flashes back through the mixing tube, a characteristic case is shown in Figure 41. In this series of instantaneous images, the flame isosurface is defined according to the reaction progress variable. Unlike temperature, the C surface is not directly affected by wall heat loss and consequently impinges on the bluff body. As the equivalence ratio increases, the flame enters the tube along the inner wall. The flame propagates upstream and tangentially with the swirling flow, prohibited from extending far beyond the boundary layer due to the high-speed streaks residing there. Additionally, the front is characterized by a series of curved bulges, inflecting toward the wall and downstream flow. Small-scale structures and wrinkles form and dissipate throughout the simulation.

The cases studied here explicitly triggered flashback, but a working combustor does see stratified flows and a potential for large periodic spikes in equivalence ratio. The sensitivity of the flame to these local increases is therefore of some consequence. While the equivalence ratio is uniformly increased at the inlet plane, the high-speed streaks carry it unevenly toward the chamber. The flame initially encounters this richer mixture near the outer radius of the mixing tube and advances, but only when the richer mixture diffuses or is convected into the boundary layer does the front flash, advancing in a manner very similar to the channel flashback. The familiar system of bulges and cusp eventually wraps around the bluff body, stretched by the swirling flow.

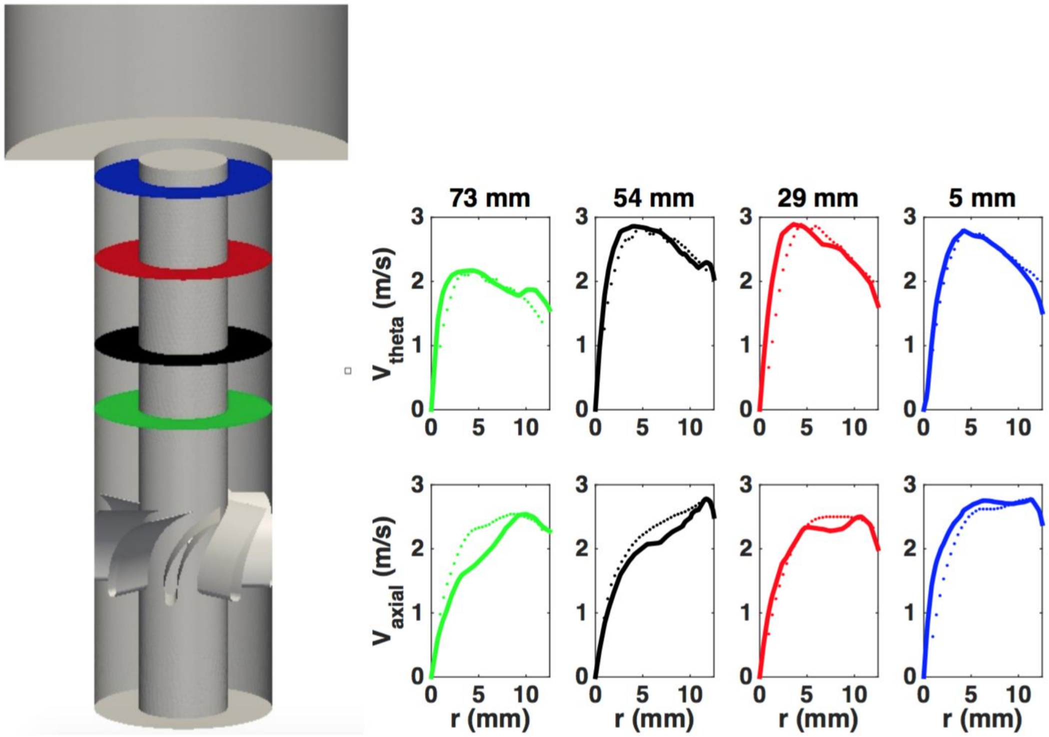

Figure 39. Time averaged streamwise and azimuthal velocity fields at four positions inside the mixing tube for LES (solid) and experiments (dotted) given a bulk velocity of 2.5 m/s. Radial position is measured from the bluff body to the outer wall while streamwise position is measured from the plane between the mixing tube and combustion chamber.

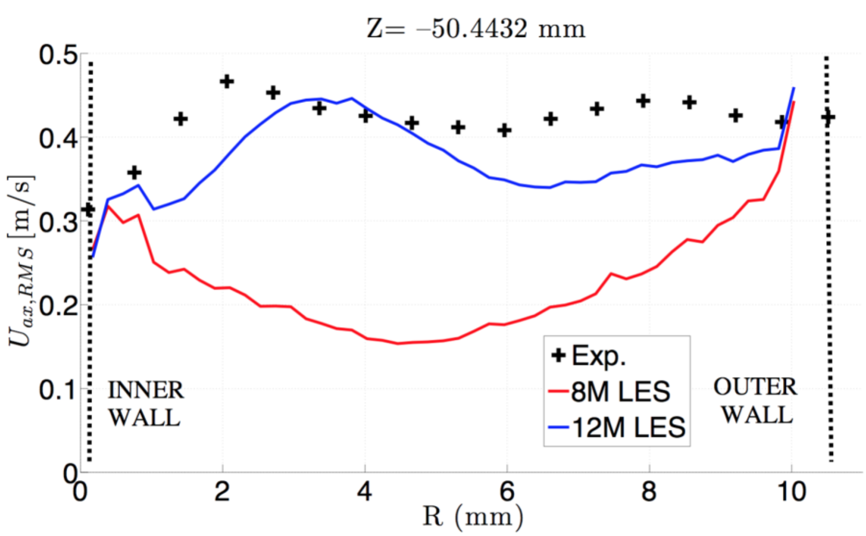

Figure 40. Root mean square (RMS) velocity near the mixing tube exit for a non-refined mesh near the vanes (solid blue line) and a refined mesh (solid red line).

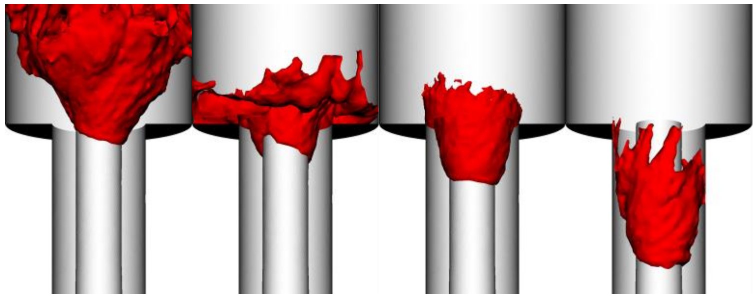

Figure 41. Instantaneous isocontours of T = 1400 K at t = 0.105 s (top left), t = 0.115 s (top right), t = 0.135 s (bottom left), and t = 0.165 s (bottom right).

While the macroscopic structure of the flame shows many of the same features of the channel flashback in the context of a swirling bulk flow, there are several differences. Considering the front shape itself, a series of ligaments extend away from the wall and out of the boundary layer. These structures are referred to in this work as flame tongues. For comparison, both the single-tongue front and the finer scale multi- tongue front are shown side by side in Figure 42. Despite reaching lengths on the order of the channel itself, these structures are characterized by short time scales, developing out of the front and rejoining it quickly. Typically present in low speed regions with locally high equivalence ratio, their overall effect on the flashback speed in minimal.

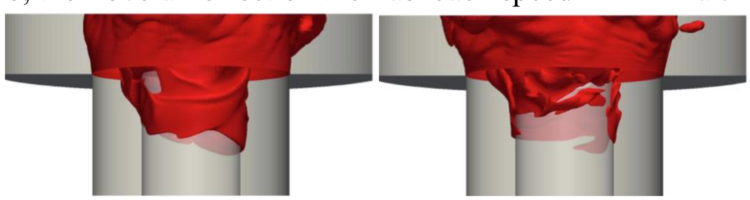

Figure 42. Instantaneous isocontours of T = 1400 K, indicating single flame tongue (top) and multi-flame tongue (bottom) behavior.

Table 1. Experimental and LES flashback speeds for both fuel compositions.

	CH4-air Flashback speed (m/s)	H2/CH4-air Flashback speed (m/s)
Experiment	0.58	0.94
LES	0.55	0.71

4.E.6 Effect of fuel variation on flame behavior and flashback speed

The results summarized in Table 1 indicate that the flashback speed varies dramatically depending upon the fuel. Experiments indicate that this is a consequence of thermo-diffusive effects and positively stretched flame tips. The hydrogen flame can approach closer to the wall before being quenched, which likely con- tributes to the higher global front propagation speed. Additionally, the pure methane flame speed is extremely well captured while the hydrogen/methane mixture flame speed is under predicted. The reasoning behind this is not immediately apparent, but upon closer inspection, many of the ideas gathered from the channel can be directly applied to explain why this discrepancy occurs.

Figure 30 shows the flame isosurface for both fuels at comparable locations. While the difference is subtle, the pure methane case is characterized by a smoother surface, while the hydrogen/methane mixture is convoluted, showing many of the same macroscopic shapes while containing small-scale corrugations over- laid. From the channel LES, it was determined that correctly resolving these small scale structures can have implications on the growth of the flame. Thermo-diffusive instability stemming from a non-unity Lewis number for the hydrogen (Law & Sung, 2000) yields a more wrinkled flame under the same Reynolds number.

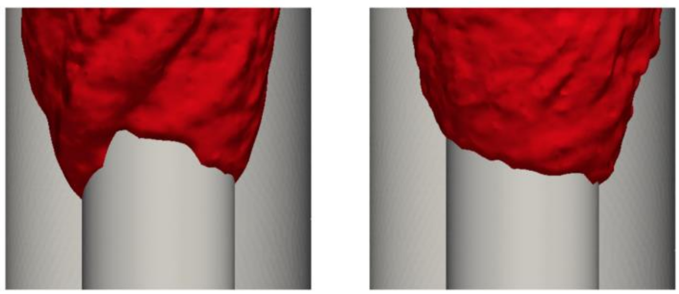

Figure 43. Instantaneous C = 0.7 isocontour for methane (left) and hydrogen/methane (right).

4.E.7 Effect of pressure on flame propagation

Consistently with the experiments conducted at UT, the effect of pressure on the flame propagation was investigated in the simulations. The flame topology is greatly affected by the pressure since the Reynolds number increases with density. Finer structures can be observed at 4 atm compared to 1 atm as illustrated in Figure 44.

The increased pressure also enhances the blockage effect induced by the flame front and therefore the density jumps throughout the flame. As a result the recirculation zone upstream the flame becomes stronger as the pressure increase (Fig. 45).

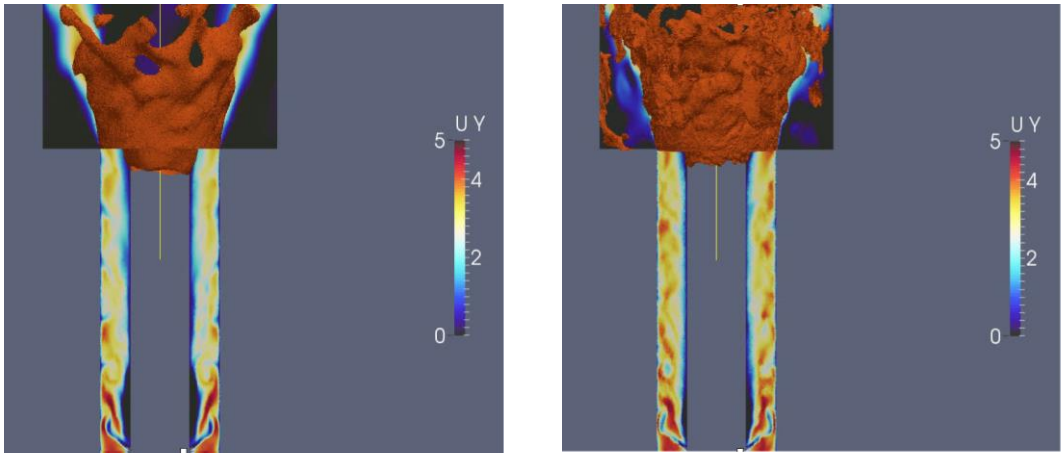

Figure 44. Instantaneous isocontours of C = 0.7 at 1 atm (left) and 4 atm (right).

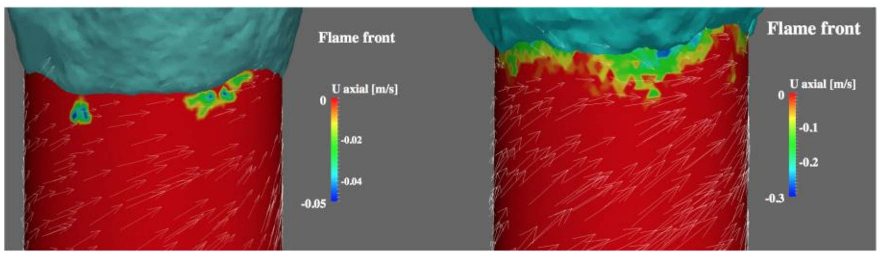

Figure 45. Instantaneous recirculation zones upstream the flame front at 1 atm (left) and 4 atm (right).

4.F Computational Program: LES of unsteady events

The results obtained in the different configuration tested give good confidence about the ability of the model to chosen to represent a single flashback realization. Although this confirms that most of the physics involved in a flashback event is well represented, it is not the kind of prediction expected for the computational tool. What is expected is rather related to the probability of witnessing a flashback given one operational condition.

4.F.1 Flashback probability prediction

In order to assess the prediction capability of the model regarding the flashback probability, a set of simulations is conducted starting from different initial conditions. The initial conditions are sampled based on the position of the precession vortex (Fig. 46) associated with the swirl. Similarly, a set of experiments started at random initial conditions is conducted. It turns out that the observed standard deviation of the mean flashback speed is much smaller in the simulations.

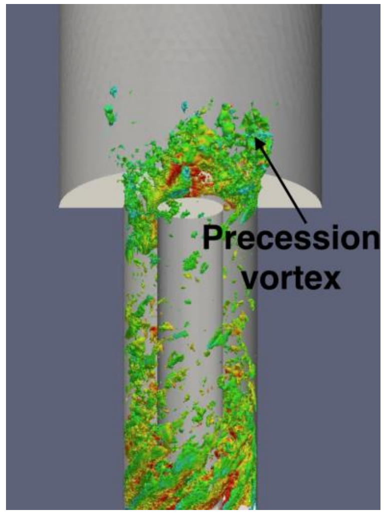

Figure 46. Precession vortex associated with the swirling flow.

Table 2. Experimental and LES variability of flashback speeds for CH4 mixture.

	Mean flashback speed	Standard Deviation
Experiment	0.58 m/s	11.3%
Simulation	0.54 m/s	0.6%

4.F.2 Statistical description of LES

Obtaining a reliable probability for flashback prediction requires describing instantaneous fields and their evolution between time steps accurately enough. Both considerations can introduce error in LES. First, multiple true fields are embedded in each filtered field. Second, only the previous time steps are used to determine the next one while the transition between time steps should be described probabilistically. Predicting unsteady combustion processes with LES requires the introduction of a statistical framework similar as what had been previously introduced for turbulence (Zandonade et al., 2004; Adrian, 1990; Pope, 2010).

4.F.2.1 Statistical evolution

The goal of a probabilistic LES approach is to capture the multi-point PDF accurately. A probabilistic evolution of field can be obtained by using a conditional mean over all possible realizations. Noting w_α the filtered velocity at point α, the evolution of the filtered field uses the other points in the system as:

$$w_\alpha(t+\Delta t) = w_\alpha(t) + \langle \frac{du}{dt} | w_1, w_2, ..., w_n \rangle \Delta t$$

The best possible solution the model can provide with LES is a conditional average of each instantaneous variable.

4.F.2.2 Subfilter modeling

For combustion modeling, subfilter scalar models should follow the same statistical approach in order to provide a reliable estimate of any probability estimation. Unresolved stress and subfilter variance have to be revisited in order to provide reasonable estimate of the field's conditional average.

For scalar variance, the Filtered Density Function (FDF) approach can be used. The statistical evolution of the Eulerian field still relies on the field's conditional average. The subfilter scalar distribution uses, on the other hand, an FDF transport equation. Noting *f* is the PDF of the scalar ψ, *w* is the filtered velocity field and $M(\psi)$ the micromixing term, the FDF transport equation takes the following form

$$\frac{\partial f}{\partial t} + \nabla \cdot (\widetilde{w f'}) = \frac{\partial}{\partial \psi}[M(\psi) f + S(\psi) f]$$

Note that the micromixing term introduces the variability required for the statistical context used here.

5 Conclusions

In this joint modeling/experimental project we have significantly improved LES modeling capability of boundary layer flashback relevant to gas-turbine combustors operating on high-hydrogen content fuels. The validation approach is to use a hierarchical approach, where the subcomponent models are validated first with simplified-physics configurations, and then the models are challenged with progressively complex physical systems. At the top of the validation pyramid is a system that includes all of the relevant physics. In this case the top of the pyramid is the experiment composed of boundary layer flashback in a lean-premixed swirl combustor at elevated pressure. An important component of this work is the companion experimental study which seeks to provide validation data that were not available in the literature at the time the grant started.

5.1 Experimental Program

In the experimental program, a new lean-premixed swirl combustor was developed. This new combustor had excellent optical access to enable a suite of high-speed laser diagnostics to be applied to it. This facility enabled measurements of flashback using CH4-air flames as well as fuel mixtures with up to 90% H_2 content. The diagnostics that were employed include kilohertz-rate chemiluminescence imaging, kilohertz-rate stereo PIV and kilohertz rate tomographic PIV. A major innovation in this work is that we developed a new technique that uses the reconstructed 3D particle fields to obtain the 3D flame surface topography. This new technique has led to new insights into the interaction between the propagating flame and the incoming boundary layer flow.

We have made some important observations regarding flame propagation. For example, we consistently observe two modes of upstream flame propagation during boundary layer flashback in swirl flows. The first mode consists of large-scale flame tongues swirling in the direction of the bulk flow as they propagate upstream. The second mode consists of small-scale flame bulges aligned with the streamwise direction, which – particularly for high-hydrogen-content flames.

The dominant mode is that which occurs with flame tongues. Flashback is led by these large-scale flame tongues swirling with the bulk flow in the azimuthal direction as they propagate upstream along the center body wall. The time-resolved planar three-component and volumetric velocity field measurements revealed that these large-scale flame tongues modify the approach flow differently. A deflection of streamlines ahead and around the flame tip causes a predominantly swirling motion including a region of negative axial velocity for the leading side of the flame tongue to propagate into. This region of negative axial velocity does not correspond to boundary layer separation or a recirculation bubble, and does not feature a stagnation point upstream of the preheat zone, as has been shown in channel-flow flashback (Eichler & Sattelmayer, 2011; Gruber et al., 2012). This is an important finding, because it shows there is a strong difference between flashback in swirling flows and nominally 2D flows such as the channel flow. The formation of the observed flame tongues affects the flow on a larger scale compared to the small-scale bulges. This observation suggests that the presumed elevated pressure region causing the streamline deflection extends well into the burnt gas.

The investigated ultra-lean high-hydrogen content flames differ from the methane flames as they are significantly more convoluted. Despite a matched laminar flame speed, small-scale bulges form and resist the approach flow more frequently. Yet during flashback events these investigated hydrogen flames are found to still form larger tongues, which propagate upstream in a swirling motion with the smaller bulges being a superimposed perturbation. These differences in the characteristics between methane and hydrogen fuels provides an important challenge for LES modeling, since the differences in flame structure seem to occur at the subfilter scale and hence must be modeled.

A more limited number of experiments were performed at pressures up to 5 atm. These studies were more limited because the experiments are much more difficult to conduct and the diagnostics are more time-consuming. Increasing pressure was shown to reduce the radial spread of the flames. It is well known that the laminar flame speed reduces at high-pressure, but the turbulent flame speed should increase by a larger factor. Therefore, the reason for this difference is not known at this time. The fact that the flame front at high pressure is considerably more turbulent and wrinkled, owing the higher Reynolds number, is also an important modeling challenge.

In summary, we have produced the most extensive experimental database to date on boundary layer flashback in a swirling flow. The measurements cover a wide-range of conditions, and the measurements are detailed enough to be suitable for validation purposes.

5.1 Computational Modeling Program

The modeling effort focused on the validation of many different submodels, as well as testing the importance of various modeling assumptions. The most important validation exercise was the use of a DNS of turbulent channel flow flashback. A large number of LES computations were used for this purpose. The LES filter widths were comparable to the smallest turbulence length scales, which would imply that the momentum description is reasonably accurate in the LES calculations. The flame, on the other hand, was approximated as a thin front using different models. In this sense, the computations were designed to test the interaction of this thin-flame assumption with the near- fully resolved flow field. The computations found certain intriguing features. The baseline case at $\Delta_{LES} = 8\Delta_{x,DNS}$ produced a flame front that is comparable in statistics to that in the DNS. Using quantities such as the depth parameter and the PDF of front fluctuations, it was found that the LES computations are very accurate in predicting the structure of the turbulent flame front. However, there was a discrepancy in the propagation velocity of the flame front. In other words, a slowly moving LES flame front was able to produce the structures of a faster moving DNS front. The flamelet-based models produced lesser variability to simulation conditions, including the choice of other subfilter models. This is expected, given that the chemical source term is the predominant quantity in the progress variable transport equation. It was found for the AFSD model that representing accurately the diffusion term was crucial to observe the characteristic flame blockage described by Gruber et al. (2012). A similar behavior for the depth and flashback velocity parameter was observed with coarse F-TACLES model.

Direct numerical simulation of flame front propagation in premixed flames was carried out, but with the added complexity of fuel stratification. For hydrogen/air flames, flame evolution in a periodic box with mean convective velocity was performed. A control algorithm to position the flame at a required streamwise location is used. It was verified that the algorithm correctly positions the flame for a one-dimensional laminar flame. The turbulent flame propagation was studied using two different inflow conditions for the scalars. When the stratification was essentially large scale dominated, the inflow was specified such that the equivalence ratio is uniform at the inlet plane but changed with time. In this case, the flame evolution was found to be similar to a succession of fully premixed flames with varying equivalence ratios. In the case when stratification occurs at the small scales, the flame front exhibits variations in peak temperature consistent with the local fuel/air ratio. Overall, the physical structure of the flame is found to be different from the large-scale stratification case.

A premixed flamelet combustion approach with F-TACLES closure model was used in LES of a swirling burner for both inert and reacting conditions. The behavior of interest was the upstream propagation of premixed methane/hydrogen flames through the low speed boundary layer. Regarding the inert validation, the simulations proved accurate: the mean velocity within the mixing tube matched the experimental results, despite some sensitivity to inflow boundary conditions. Furthermore, macroscopic flow features such as high-speed streaks, vortex breakdown, and a precessing vortex core were also well represented.

An important result of this project is to clarify what is meant by a “predictive” simulation of flashback. Specifically, using the combustion models described in Sec. 4.C.2.1 enables us to reasonably accurate prediction of flashback velocity. However, in the actual context of flashback prediction, the model also has to be as sensitive as the experimental set-up to accurately represent the variability associated with the event. For example, if the real device has greater sensitivity to variable inlet temperature than the LES model, then the simulation will likely not be able to predict flashback under actual operating conditions. Using LES for such problems requires a careful definition of the statistics that LES can provide. Subfilter stress and scalar variance models have to be revisited for coherence with the probabilistic point of view adopted.

6 Appendix – Control algorithm for flame placement

In order to ensure that the flame encounters the same turbulent flow statistics for the entire duration of the simulation, its position is controlled using a control algorithm. The control algorithm relies on introducing a correction velocity at the inflow to counter flame motion away from the control point. The procedure is based on the algorithm introduced by Bell et al. (2006). In this work, a controller with a static gain equal to 1 is used. The control block is show in Fig. A.1.

Recognizing that the local elementary variation of the flame position can be written in terms of the local flow velocity and the local flame velocity as can derive this control procedure

$$\Delta h = (U_{in} - s_T)dt$$

where h is the flame position, U_{in} is the local flow velocity encountered by the flame front and s_T is the local turbulent flame velocity. For use in the control algorithm, a response time τ is defined. This time should be interpreted as the time between the moment where the convection velocity correction is applied and the moment where the flame position is effectively corrected. This response time τ is expressed in terms of the simulation time step as

$$\tau = K\Delta t$$

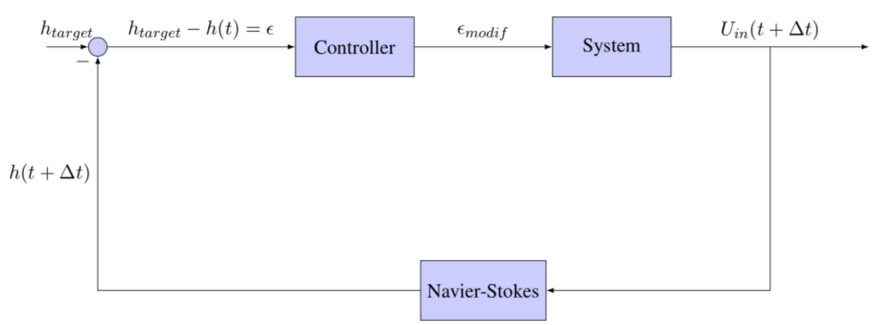

Figure A.1. Block diagram describing the control loop.

where Δt is the simulation time step and K is a constant greater than 1. It was found that values of K close to 4 gave stable and accurate results. Based on this response time, the convective velocity to impose at the inlet is simply expressed by

$$U_{in}(t + \Delta t) = 2\frac{\epsilon}{K^2\Delta t} - 2\frac{\Delta h}{K\Delta t} + U_{in}(t)$$

where ε is the difference between the intended flame location (in x distance) and the current flame location. In the above equation, the first term of the right hand side is the contribution of the global error in the flame position. The second term is the contribution of the instantaneous variation of the flame position. It can be seen from Eq. 7 that those two contributions have opposite sign. Thus, as the flame gets closer from the target position, the correction is progressively damped which reduces the flame oscillations around the target position. Note also that since K > 1, the dominant term of the convective velocity correction is due to the instantaneous flame position variation. The convective velocity is then actively corrected at each time step. It is therefore important to generate turbulent inflow independent of the mean convective velocity (described in Sec. 7.1). The formula presented for the control algorithm does not explicitly require an estimation of the turbulent flame velocity. However, this quantity can be easily obtained by,

$$s_T = U_{in}(t) - \frac{\Delta h}{\Delta t}$$

To validate the algorithm used here, a 1D flame configuration with detailed chemistry has been simulated. A premixed hydrogen/air mixture with equivalence ratio of 0.55 is used. The inlet temperature is set to 750 K and the configuration operates at 2 atm. For this configuration, the expected laminar flame speed is 6.67 m/s as obtained from a one-dimensional steady calculation using the FlameMaster code (Pitsch). The flame is initialized at X = 15 mm and the target flame position is X = 7.5 mm. By intentionally initializing the flame at a location other than the set point, it is possible to understand the efficiency of the algorithm in controlling the flame position. The flame is resolved using the same number of points as in the full-scale DNS described in Sec. 7.1.

Figure A.2 shows the specified convection velocity at the inlet based on the control algorithm and the variation in the estimated flame velocity. In the first few time-steps, the flame propagates towards the target position. During this time, the control velocity is set to zero since the flame is moving upstream towards the set point. When the flame is close to the set location, the control velocity starts to increase to prevent the flame from propagating further upstream. After that, the damping algorithm ensures that the flame does not move too far from the set point, and the control velocity finally reaches the asymptotic value close to the laminar flame speed.

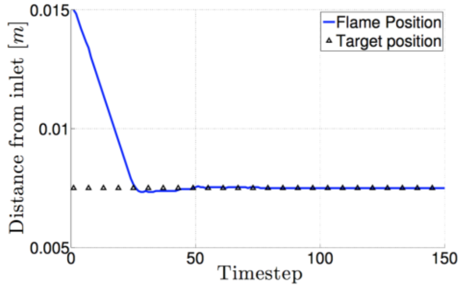

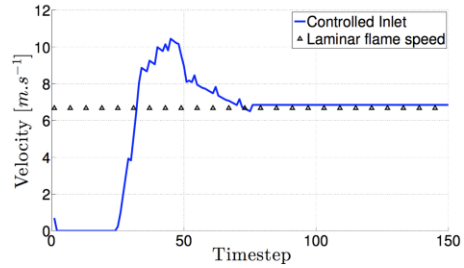

Figure A.2. Variation of (left) flame position and (right) inlet velocity, with time.

7 References

Adrian, R. J., "Stochastic estimation of sub-grid scale motions," *Applied Mechanics Reviews*, Vol. 43, 1990, pp. 214–218.

Akselvoll, K. and Moin, P., "Large Eddy Simulation of Turbulent Confined Coannular Jets," *Journal of Fluid Mechanics*, Vol. 315, 1996, pp. 387–411.

Ashurst, W.T., "Flame Propagation Along a Vortex: the Baroclinic Push," *Combust. Sci. Technol.*, 112 (1996) 175–185.

Auzillon, P., Fiorina, B., Vicquelin, R., Darabiha, N., Gicquel, O., and Veynante, D., "Modeling chemical flame structure and combustion dynamics in LES," *Proceedings of the Combustion Institute*, Vol. 33, 2011, pp. 1331–1338.

Bell, J. B., Day, M. S., Grcar, J. F., and Lijewski, M. J., "Active control for statistically stationary turbulent premixed flame simulations," *Communications in Applied Mathematics and Computational Science*, Vol. 1, 2006, pp. 29–51.

Boger, M., Veynante, D., Boughanem, H., and Trouve, A., "Direct numerical simulation analysis of flame surface density concept for large eddy simulation of turbulent premixed combustion," *Twenty- Seventh Symposium (International) on Combustion*, Vol. 27, 1998, pp. 917–925.

Colin, F., Ducros, F., Veynante, D., and Poinsot, T., "A Thickened Flame Model for Large-Eddy Sim- ulation of Premixed Turbulent Combustion," *Physics of Fluids*, Vol. 12, No. 7, 2000, pp. 1843–1863.

Curtiss, C.F. and Hirschfelder, J.O., "Transport Properties of Multicomponent Gas Mixtures," *Journal of Chemical Physics*, Vol. 17, 1949, pp. 550.

de Swart, J.A.M., Bastiaans, J.M., van Oijen, J.A., de Goey, L.P.H., and Cant, R.S., "Inclusion of Preferential Diffusion in Simulations of Premixed Combustion of Hydrogen/Methane Mixtures with Flamelet Generated Manifolds," *Flow Turbulence and Combustion*, Vol. 85, 2010, pp. 473–511.

Ebi, D. and Clemens, N.T., "Time-Resolved PIV and Flame Front Imaging of Boundary Layer Flashback in a Swirl Combustor", 17th International Symposium on Application of Laser Techniques to Fluid Mechanics, Portugal, July 7-10, 2014

Eichler, C. and Sattelmayer, T., "Experiments on Flame Flashback in a Quasi-2D

Turbulent Wall Boundary Layer for Premixed Methane-Hydrogen-Air Mixtures," *J. Eng. Gas Turbines Power*, 133 (2011) 011503.

Eswaran, V. and Pope, S. B., "Direct Numerical Simulations of the Turbulent Mixing of a Passive Scalar," *Physics of Fluids*, Vol. 31, 1988, pp. 506.

Felten, F. N. and Lund, T. S., "Kinetic energy conservation issues associated with the collocated mesh scheme for incompressible flow," *Journal of Computational Physics*, Vol. 215, 2006, pp. 465–484.

Fiorina, B., Vicquelin, R., Auzillon, P., Darabiha, N., Gicquel, O., and Veynante, D., "A filtered tab- ulated chemistry model for LES of premixed combustion," *Combustion and Flame*, Vol. 157, 2010, pp. 465–475.

Gruber, A., Chen, J. H., Valiev, D., and Law, C. K., "Direct numerical simulation of premixed flame boundary layer flashback in turbulent channel flow," *Journal of Fluid Mechanics*, Vol. 709, 2012, pp. 516–542.

Ham, F. and Iaccarino, G., "Energy conservation in collocated disretization schemes on unstructured meshes," *CTR Annual Research Briefs*, 2004.

Heeger, C., Gordon, R.L., Tummers, M.J., Sattelmayer, T. and Dreizler, A., "Experimental analysis of flashback in lean premixed swirling flames: upstream flame propagation," *Exp. Fluids,* 49 (2010) 853–863.

Hergart, C. and Peters, N., "Applying the representative interactive flamelet model to evaluate the potential effect of wall heat transfer on soot emissions in a small-bore direct-injection diesel engine," *Journal of engineering for gas turbines and power-transactions of the ASME*, Vol. 124, 2002, pp. 1042–1052.

Hernandez-Perez, F., Yuen, F., Groth, C., and Gulder, O., "LES of a laboratory-scale turbulent pre- mixed bunsen flame using FSD, PCM-FPI, and thickened flame models," *Proceedings of the Combus- tion Institute*, Vol. 33, 2011, pp. 1365–1371.

Issa,R.I.,"SolutionoftheImplicitlyDiscretisedFluidFlowEquationsbyOperator-Splitting,"*Journal of Computational Physics*, Vol. 62, 1985, pp. 40–65.

Karimi, N., Heeger, C., Christodoulou, L. and Dreizler, A., "Experimental and Theoretical Investigation of the Flashback of a Swirling, Bluff-Body Stabilised, Premixed Flame," *Zeitschrift Für Phys. Chemie*, 229 (2015) 663–689.

Kiesewetter, F, Konle, M., Sattelmayer, T., "Analysis of Combustion Induced Vortex Breakdown Driven Flame Flashback in a Premix Burner With Cylindrical Mixing Zone," *J. Eng. Gas Turbines Power*, 129 (2007) 929–936.

Konle, M. and Sattelmayer, T., "Interaction of heat release and vortex breakdown during flame flashback driven by combustion induced vortex breakdown," *Exp. Fluids*, 47 (2009) 627–635.

Konle, M., Kiesewetter, F. and Sattelmayer, T., "Simultaneous high repetition rate PIV–LIF-measurements of CIVB driven flashback," *Exp. Fluids*, 44 (2008) 529–538.

Kravchenko, A. G. and Moin, P., "On the Effect of Numerical Errors in Large Eddy Simulations of Turbulent Flows," *Journal of Computational Physics*, Vol. 131, 1997, pp. 310–322.

Law, C. K. and Sung, C., "Structure, aerodynamics, and geometry of premixed flamelets," *Progress In Energy and Combustion Science*, Vol. 26, 2000, pp. 459–505.

Li, J., Zhao, Z., Kazakov, A., and Dryer, F., "An updated comprehensive kinetic model of hydrogen combustion," *International Journal of Chemical Kinetics*, Vol. 36, 2004, pp. 566–575.

Lundgren, T. S., "Linearly forced isotropic turbulence," *Annual Research Briefs*, 2003, pp. 461–473.

Mahesh, K., Constantinescu, G., and Moin, P., "A Numerical Method for Large-Eddy Simulation in Complex Geometries," *Journal of Computational Physics*, Vol. 197, 2004, pp. 215–240.

Menon, S. K., Boettcher, P. A., and Blanquart, G., "Enthalpy based approach to capture heat transfer effects in premixed combustion," *Combustion and Flame*, Vol. 160, 2013, pp. 1242–1253.

Mercier, R., Auzillon, P. and Moureau, V., "LES Modeling of the Impact of Heat Losses and Differential Diffusion on Turbulent Stratified Flame Propagation: Application to the TU Darmstadt Stratified Flame," *Flow Turbulence and Combustion*, Vol. 93, 2014, pp. 349–381.

Morinishi, Y., "Skew-symmetric form of convective terms and fully conservative finite difference schemes for variable density low-Mach number flows," *Journal of Computational Physics*, Vol. 229, 2010, pp. 276–300.

Mueller, M. E. and Pitsch, H., "LES model for sooting turbulent nonpremixed flames," *Combustion and Flame*, Vol. 159, 2012, pp. 2166–2180.

Nauert, A, Petersson, P., Linne, M. and Dreizler, A., "Experimental analysis of flashback in lean premixed swirling flames: conditions close to flashback," *Exp. Fluids,* 43 (2007) 89–100.

Pierce, C. D. and Moin, P., "Progress-variable Approach for Large-Eddy Simulation of Non-Premixed Turbulent Combustion," *Journal of Fluid Mechanics*, Vol. 504, 2004, pp. 73–97.

Pitsch, H., "A C++ Computer Program for 0-d and 1-D Laminar Flame Calculations," RWTH Aachen.

Pope, S. B., "Self-conditioned fields for large-eddy simulations of turbulent flows," *Journal of Fluid Mechanics*, Vol. 652, 2010, pp. 139–169.

Rosales, C. and Meneveau, C., "Linear forcing in numerical simulations of isotropic turbulence: Physical space implementations and convergence properties," *Physics of Fluids*, Vol. 17, 2005.

Shunn, L., Ham, F., and Moin, P., "Verification of variable-density flow solvers using manufactured solutions," *Journal of Computational Physics*, Vol. 231, 2012, pp. 3801–3827.

Tabor, G. and Weller, H., "Large eddy simulation of premixed turbulent combustion using xi-flame surface wrinkling model," *Flow, Turbulence and Combustion*, Vol. 72, 2004, pp. 1–28.

Tangermann, E. and Pfitzner, M., "Evaluation of combustion models for combustion-induced vortex breakdown," *Journal of Turbulence*, Vol. 10, No. 7, 2009, pp. 1–21.

Trisjono, P., Kleinheinz, K., Kang, S., & Pitsch, H., "Large Eddy Simulation of Stratified and Sheared Flames of a Premixed Turbulent Stratified Flame Burner Using a Flamelet Model with Heat Loss," *Flow Turbulence and Combustion*, Vol. 92, 2014, pp. 201–235.

Zandonade, P. S., Langford, J. A., and Moser, R. D., "Finite-volume optimal large-eddy simulation of isotropic turbulence," *Physics of fluids*, Vol. 16, No. 7, 2004, pp. 2255–2271.

8 Bibliography – Publications resulting from this work

1. Ebi, D. and Clemens, N.T., *Experimental investigation of upstream flame propagation during boundary layer flashback of swirl flames*, Combustion and Flame, to be published, 2016.

2. Ebi, D. and Clemens, N.T., *Simultaneous high-speed 3D flame front detection and tomographic PIV*, Measurement Science and Technology, to be published, 2016.

3. Y. Tang, M. Hassanaly, H. Koo, V. Raman, *Large eddy simulation of flame stabilization in a multi-jet burner using a non-adiabatic flamelet approach* 54th AIAA Aerospace Sciences Meeting, 2016.

4. M. Hassanaly, V. Raman, *Large Eddy Simulation of unsteady combustion events*, 13th US National Congress on Computational Mechanics, 2015.

5. C. Lietz, Y. Tang, M. Hassanaly, H. Koo, V. Raman, *LES of a high-pressure multi-jet combustor using FPVA* 10th OpenFOAM Workshop, 2015.

6. Ebi, D., Ranjan, R. and Clemens, N.T., "Experimental investigation of swirl flame boundary-layer flashback at elevated pressure," 9th US National Combustion Meeting, Cincinnati, Ohio, May 2015.

7. Ebi, D. and Clemens, N.T., "Flow-flame interaction in turbulent boundary layer flashback of swirl flames," 9th International Symposium on Turbulence and Shear Flow Phenomena, Melbourne, Australia, June 2015.

8. M. Hassanaly, H. Koo, V. Raman, *Effect of compressibility in the flashback of premixed flames in confined channels*, 15th International Conference on Numerical Combustion, 2015.

9. M. Hassanaly, V. Raman, H. Koo, M. B. Colket, Influence of Fuel Stratification on Turbulent Flame Propagation 53rd AIAA Aerospace Sciences Meeting, 2015.

10. C. Lietz, M. Hassanaly, V. Raman, *Large Eddy Simulation of Flame Flashback in Swirling Premixed CH4/H2-Air Flames* 53rd AIAA Aerospace Sciences Meeting, 2015.

11. M. Hassanaly , C. Lietz , V. Raman, H. Kolla, J. Chen, A. Gruber, *Large Eddy Simulation of premixed flame flashback in a turbulent channel*, 67th Annual Meeting of the APS Division of Fluid Dynamics, 2014.

12. C. Lietz , M. Hassanaly , V. Raman, H. Kolla, J. Chen, A. Gruber, *Large Eddy Simulation of premixed flame flashback in a turbulent channel*, 52nd AIAA Aerospace Sciences Meeting, 2014.

13. Ebi, D. and Clemens, N.T., "Time-resolved PIV and flame front imaging of boundary layer flashback in a swirl combustor," 17th International Symposium on Application of Laser Techniques to Fluid Mechanics, Lisbon, Portugal, July 7-10, 2014.

14. Ebi, D. and Clemens, N.T., "Experimental investigation of flashback in premixed CH4/H2-air swirl flames," paper AIAA 2013-2604, 43rd Fluid Dynamics Meeting, June 2013.

15. Ebi, D. and Clemens, N.T., "Experimental investigation of flashback mechanism in premixed high-hydrogen-content swirl flames," The Fall Meeting of the Western States Section of the Combustion Institute, October 7-8, 2013.

9 Acronyms

3D	three dimensional
AFSD	algebraic flame surface density
CMOS	complementary metal oxide semi-conductor
DF	direct flamelet
DNS	direct numerical simulation
FDF	filtered density function
F-TACLES	filtered tabulated chemistry for large eddy simulation
LES	large-eddy simulation
LSS	large-scale stratification
Nd:YLF	Neodymium: Yttrium Lithium Fluoride
PIV	particle image velocimetry
SSS	small-scale stratification